



1           Ammonium CI-Orbitrap: a tool for characterizing the  
2                            reactivity of oxygenated organic molecules

3   Dandan Li<sup>1</sup>, Dongyu Wang<sup>2</sup>, Lucia Caudillo<sup>3</sup>, Wiebke Scholz<sup>4</sup>, Mingyi Wang<sup>5,6</sup>, Sophie Tomaz<sup>1</sup>,  
4   Guillaume Marie<sup>3</sup>, Mihnea Surdu<sup>2</sup>, Elias Eccli<sup>4</sup>, Xianda Gong<sup>7</sup>, Loic Gonzalez-Carracedo<sup>8</sup>, Manuel  
5   Granzin<sup>3</sup>, Joschka Pfeifer<sup>3,9</sup>, Birte Rörup<sup>10</sup>, Benjamin Schulze<sup>6</sup>, Pekka Rantala<sup>10</sup>, Sébastien Perrier<sup>1</sup>,  
6   Armin Hansel<sup>4</sup>, Joachim Curtius<sup>3</sup>, Jasper Kirkby<sup>3,9</sup>, Neil M. Donahue<sup>5</sup>, Christian George<sup>1</sup>, Imad El-  
7   Haddad<sup>2</sup>, Matthieu Riva<sup>1,\*</sup>

8   <sup>1</sup> Univ Lyon, Université Claude Bernard Lyon 1, CNRS, IRCELYON, 69626, Villeurbanne, France

9   <sup>2</sup> Laboratory of Atmospheric Chemistry, Paul Scherrer Institute, 5232, Villigen, Switzerland

10   <sup>3</sup> Institute for Atmospheric and Environmental Sciences, Goethe University Frankfurt, 60438,  
11   Frankfurt am Main, Germany

12   <sup>4</sup> Institute for Ion Physics and Applied Physics, University of Innsbruck, 6020, Innsbruck, Austria

13   <sup>5</sup> Center for Atmospheric Particle Studies, Carnegie Mellon University, Pittsburgh, PA, 15213, USA

14   <sup>6</sup> Division of Chemistry and Chemical Engineering, California Institute of Technology, Pasadena, CA  
15   91125, USA

16   <sup>7</sup> Leibniz Institute for Tropospheric Research, 04318, Leipzig, Germany

17   <sup>8</sup> Faculty of Physics, University of Vienna, Vienna, 1090, Austria

18   <sup>9</sup> CERN, the European Organization for Nuclear Research, CH-1211 Geneve 23, Switzerland

19   <sup>10</sup> Institute for Atmospheric and Earth System Research/Physics, Faculty of Science, University of  
20   Helsinki, 00014, Helsinki, Finland

21

22   \* Email: [matthieu.riva@ircelyon.univ-lyon1.fr](mailto:matthieu.riva@ircelyon.univ-lyon1.fr)



23 Abstract

24 Oxygenated organic molecules (OOMs) play an important role in the formation of atmospheric  
25 aerosols. Due to various analytical challenges in measuring organic vapors, uncertainties remain in the  
26 formation and fate of OOMs. The chemical ionization Orbitrap mass spectrometer (CI-Orbitrap) has  
27 recently been shown to be a powerful technique able to accurately identify gaseous organic  
28 compounds due to its great mass resolving power. Here we present the ammonium ion ( $\text{NH}_4^+$ ) based  
29 CI-Orbitrap as a technique capable of measuring a wide range of gaseous OOMs. The performance of  
30 the CI- $(\text{NH}_4^+)$ -Orbitrap was compared with that of state-of-the-art mass spectrometers, including a  
31 nitrate ion ( $\text{NO}_3^-$ ) based CI coupled to an atmospheric pressure interfaced to long time-of-flight mass  
32 spectrometer (APi-LTOF), a new generation of proton transfer reaction-TOF mass spectrometer  
33 (PTR3-TOF), and an iodide ( $\text{I}^-$ ) based CI-TOF mass spectrometer equipped with a Filter Inlet for  
34 Gases and AEROSols (FIGAERO-CIMS). The instruments were deployed simultaneously in the  
35 Cosmic Leaving OUTdoors Droplets (CLOUD) chamber at the European Organization for Nuclear  
36 Research (CERN) during the CLOUD14 campaign in 2019. Products generated from  $\alpha$ -pinene  
37 ozonolysis across multiple experimental conditions were simultaneously measured by the mass  
38 spectrometers.  $\text{NH}_4^+$ -Orbitrap was able to identify the widest range of OOMs (i.e.,  $\text{O} \geq 2$ ), from low  
39 oxidized species to highly oxygenated volatile organic compounds (HOM). Excellent agreements were  
40 found between the  $\text{NH}_4^+$ -Orbitrap and the  $\text{NO}_3^-$ -LTOF for characterizing HOMs and with the PTR3-  
41 TOF for the less oxidized monomeric species. A semi-quantitative information was retrieved for  
42 OOMs measured by  $\text{NH}_4^+$ -Orbitrap using calibration factors derived from this side-by-side  
43 comparison. As other mass spectrometry techniques used during this campaign, the detection  
44 sensitivity of  $\text{NH}_4^+$ -Orbitrap to OOMs is greatly affected by relative humidity, which may be related to  
45 changes in ionization efficiency and/or multiphase chemistry. Overall, this study shows that  $\text{NH}_4^+$  ion-  
46 based chemistry associated with the high mass resolving power of the Orbitrap mass analyzer can  
47 measure almost all-inclusive compounds. As a result, it is now possible to cover the entire range of  
48 compounds, which can lead to a better understanding of the oxidation processes.

49



## 50 1 Introduction

51 Aerosols affect the climate by either directly scattering or absorbing solar radiation, or acting as seeds  
52 for cloud formation (Fan et al., 2016; Haywood and Boucher, 2000). A major fraction of submicron  
53 aerosol mass consists of organic compounds, with secondary organic aerosol (SOA) predominating  
54 (Jimenez et al., 2009; Hallquist et al., 2009). Oxygenated organic molecules (OOMs) generated from  
55 the oxidation of volatile organic compounds (VOCs) contribute to the formation and growth of SOA  
56 (Ehn et al., 2014; Mellouki et al., 2015). OOMs can be generated by the autoxidation of peroxy radical  
57 ( $\text{RO}_2$ ) (Bianchi et al., 2019), where  $\text{RO}_2$  undergoes an intramolecular H atom shift, followed by  $\text{O}_2$   
58 addition forming a new and more oxidized  $\text{RO}_2$  (Crouse et al., 2013; Rissanen et al., 2014; Bianchi et  
59 al., 2019). These propagation steps are repeated until termination occurs by either bimolecular or  
60 unimolecular reactions, yielding closed-shell molecules (Bianchi et al., 2019). Among the OOMs, the  
61 highly oxygenated organic molecules (HOMs), containing multiple functional groups and exhibiting  
62 (extremely) low saturation vapor pressure, can nucleate in concert with inorganic species e.g., sulfuric  
63 acid or on their own (Ehn et al., 2014; Kirkby et al., 2016; Bianchi et al., 2016), forming new particles.  
64 Less oxygenated molecules (i.e., containing 2 to 5 oxygen atoms) play a vital role in the growth of  
65 newly formed atmospheric particles, either by condensation or through multiphase chemistry (Bianchi  
66 et al., 2019; Ehn et al., 2014; Hallquist et al., 2009). Therefore, the identification and quantification of  
67 the wide diversity of OOMs are essential to understand SOA formation and growth (Kirkby et al.,  
68 2016; Bianchi et al., 2016; Trostl et al., 2016; Jokinen et al., 2015; Glasius and Goldstein, 2016).

69 Mass spectrometry (MS) has made remarkable achievements in detecting, characterizing, and  
70 quantifying OOMs (Wang et al., 2017; Wang et al., 2020; Breitenlechner et al., 2017; Bianchi et al.,  
71 2019; Ehn et al., 2010; Riva et al., 2019a; Breitenlechner et al., 2017). Moreover, the application of  
72 chemical ionization (CI) enables the detection of a wide variety of organic and inorganic analytes  
73 (Bianchi et al., 2019; Ehn et al., 2014; Jokinen et al., 2012; Lee et al., 2014). However, the selection of  
74 ionization chemistry in combination with MS detection technique will impact the methods selectivity  
75 and sensitivity toward certain groups of OOMs (Bianchi et al., 2019; Riva et al., 2020; Riva et al.,  
76 2019b; Berndt et al., 2018b; Berndt et al., 2018a). For example, negative ion-based chemistry,  
77 including nitrate ( $\text{NO}_3^-$ ), can optimally detect HOMs, which only constitute a small subset of the  
78 OOMs (Lee et al., 2014; Berndt et al., 2015; Berndt et al., 2018b; Riva et al., 2019b). Positive ion-  
79 based chemistries have also been developed, showing great sensitivity to HOMs as well as less  
80 oxidized products, providing the possibility of achieving carbon closure of the OOMs (Praplan et al.,  
81 2015; Berndt et al., 2018a; Berndt et al., 2018b; Hansel et al., 2018; Riva et al., 2020; Riva et al.,  
82 2019b). However, these positive ion methods are mainly based on proton transfer and often result in  
83 fragmentation of the analytes (Yuan et al., 2017; Breitenlechner et al., 2017; Li et al., 2020). Time-of-  
84 flight (TOF) mass spectrometers using ammonium ( $\text{NH}_4^+$ ) or amines as reagent ions can detect a wide  
85 variety of OOMs but suffer from a lack of mass resolving power, making peak identification  
86 challenging, especially for complex systems, i.e., under ambient conditions (Berndt et al., 2018b;  
87 Berndt et al., 2018a; Riva et al., 2019b). Finally, the recently developed Orbitrap mass spectrometer  
88 using propylamine has achieved unambiguous identification of overlapping peaks and accurate



89 quantification of OOMs (Riva et al., 2019a). However, this analytical technique has been used in very  
90 diluted and dry environments to ensure a linear response to the OOMs produced from simple  
91 atmospheric systems, i.e., a single VOC precursor and oxidant (Riva et al., 2020; Riva et al., 2019b).

92 Here, we explore the capability of  $\text{NH}_4^+$  ion-based CI-Orbitrap mass spectrometer (Q-Exactive  
93 Orbitrap, Thermo Scientific) for detecting OOMs generated from  $\alpha$ -pinene ozonolysis in the Cosmic  
94 Leaving OUtdoors Droplets (CLOUD) chamber at the European Organization for Nuclear Research  
95 (CERN) under various environmental conditions. We compare the performance of the CI- $(\text{NH}_4^+)$ -  
96 Orbitrap to state-of-the-art online mass spectrometers including a nitrate CI atmospheric pressure  
97 interface long time of flight mass spectrometer (CI- $(\text{NO}_3^-)$ -APi-LTOF; Tofwerk AG), a proton transfer  
98 reaction time of flight mass spectrometer (PTR3-TOF; Ionicon Analytik GmbH), and an iodide CI  
99 time of flight mass spectrometer equipped with a Filter Inlet for Gases and AEROSols (I<sup>-</sup>-FIGAERO-  
100 CIMS, Tofwerk AG).

## 101 **2 Experimental approach and product analysis**

### 102 **2.1 CLOUD chamber experiments**

103 All experiments were conducted in the CLOUD chamber, a 26 m<sup>3</sup> cylindrical stainless-steel vessel at  
104 CERN. The chamber can achieve a pristine background for the study of nucleation (Kirkby et al.,  
105 2011; Kirkby et al., 2016). The chamber operated as a continuously stirred tank reactor (CSTR), with  
106 mixing driven by two inductively coupled fans at the top and bottom of the chamber. Evaporated  
107 liquid nitrogen ( $\text{N}_2$ ) and liquid oxygen ( $\text{O}_2$ ) were blended at a ratio of 79:21 to provide ultra-pure  
108 synthetic air, which flushed the chamber constantly. Variable amounts of trace gases, including  $\text{O}_3$ ,  
109 VOCs,  $\text{NO}_x$ ,  $\text{SO}_2$ , and CO were accurately injected into the chamber via a gas control system and  
110 monitored. Photolysis was driven by various light sources, including Hg-Xe UV lamps, and UV  
111 excimer laser. Between experiments, the chamber was cleaned by irrigating the walls with ultra-pure  
112 water, then heated to 373 K, and flushed with humidified pure air and high ozone, reducing the  
113 contaminant (e.g., VOCs) to sub pptv levels. During the cleaning process, particles were removed  
114 using a high-voltage electric field.

115 The results presented here were from the CLOUD14 campaign performed in autumn 2019.  
116 During CLOUD14, the total flow was kept at 250 standard liters per minute (slpm), providing an  
117 average residence time of 104 minutes.  $\alpha$ -Pinene was introduced into the chamber by passing a small  
118 flow of dry air over a temperature-controlled evaporator containing liquid  $\alpha$ -pinene. Ozone was  
119 generated by flowing a small fraction of the air through a quartz tube surrounded by UVC lights  
120 (wavelength < 240 nm). Experiments were performed at low temperature ( $263 \pm 0.1$  K). The RH in the  
121 chamber was controlled by flowing a portion of the air through a Nafion® humidifier using ultrapure  
122 water (18 M $\Omega$  cm, Millipore Corporation). The contents of the chamber were monitored by a wide  
123 range of external instruments connected to the sampling probes that protrude ~1 m into the chamber.

124

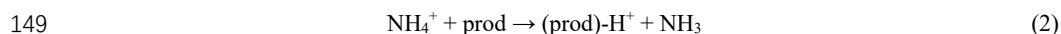
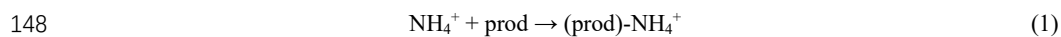


## 125 2.2 Product analysis by CI-(NH<sub>4</sub><sup>+</sup>)-Orbitrap

126 The chemical composition of closed-shell molecules was determined in real time by means of a CI-  
127 Orbitrap sampling from the CLOUD chamber through a 750 mm long, 10 mm inner diameter Teflon  
128 tube at a flow rate of 10 slpm. The CI inlet mounted on the Orbitrap was custom-built with minor  
129 modifications from the commercial inlet (Riva et al., 2019a). The ion-molecule reaction (IMR)  
130 proceeded at atmospheric pressure with a residence time of 200-300 ms. The same operating  
131 parameters used in our previous studies (RF level 60, automatic gain control  $1 \times 10^6$  charges,  
132 maximum injection time 1000 ms, multi RF ratio 1.2, mass resolution  $m/\Delta m$  140,000 at  $m/z$  200),  
133 were used, thereby minimizing declustering and maximizing the linearity range (Riva et al., 2019a;  
134 Riva et al., 2020; Cai et al., 2022).

135 The high resolution Orbitrap mass spectra data were analyzed using “Orbitool” software with a  
136 graphical user interface (GUI) (<https://orbitrap.catalyse.cnrs.fr>) (Cai et al., 2021). The analysis  
137 procedures included data averaging, noise determination and reduction, single peak fitting, mass  
138 calibration, assignment of molecular formulas, and export of time series. Signals were averaged over  
139 5 min before determining the noise and performing mass calibration.

140 NH<sub>4</sub><sup>+</sup> has been utilized in proton-transfer reaction mass spectrometry (PTR-MS) (Lindinger et al.,  
141 1998; Berndt et al., 2018b; Hansel et al., 2018). Here, this ionization technique was used to detect  
142 OOMs and was operated in a similar fashion as in our initial study (Riva et al., 2019a). NH<sub>3</sub> was added  
143 into the ion source by flushing 2 sccm of dry air over the headspace of a 1% liquid ammonia water  
144 mixture (prepared from a MilliQ water and a 25% ammonium hydroxide stock solution, ACS reagent,  
145 Sigma-Aldrich). The product molecules (“prod”) were softly charged by binding to ammonium (NH<sub>4</sub><sup>+</sup>)  
146 ions, forming (prod)-NH<sub>4</sub><sup>+</sup> adduct ions or protonated products (prod)-H<sup>+</sup>, following either reaction (1)  
147 or (2),



150 Direct detection of the NH<sub>4</sub><sup>+</sup> reagent ion cannot be detected due to the cut-off of the Orbitrap  
151 mass analyzer (i.e,  $m/Q$  50). Due to the absence of a reagent ion signal normalization of the raw  
152 analyte signal is difficult and hinders quantification of OOMs. However, we observed a total of 62  
153 peaks corresponding to amines, including C<sub>4</sub>H<sub>12</sub>N<sup>+</sup>, and C<sub>6</sub>H<sub>14</sub>N<sup>+</sup>, which are formally ammonia  
154 derivatives. To some extent, their signals can be used to correct for changes in NH<sub>4</sub><sup>+</sup> ion chemistry.  
155 Among these peaks, 13 were abundant and constant throughout the measurement period (Fig. S1). As  
156 a result, these signals were used as surrogates for the primary reagent ion signal to normalize the  
157 signal intensity of the analytes and to account for the potential variation of the ionization process  
158 (Riva et al., 2019b).

159 The concentrations of OOMs, including monomeric species such as C<sub>10</sub>H<sub>14</sub>O<sub>x</sub> and C<sub>10</sub>H<sub>16</sub>O<sub>x</sub>,  
160 were estimated based on correlation analysis between NH<sub>4</sub><sup>+</sup>-Orbitrap and NO<sub>3</sub><sup>-</sup>-LTOF/PTR3-TOF for  
161 species with the same elemental composition, providing semi-quantitative measurements. Compounds



162 with a Pearson correlation coefficient greater than 0.9 were used to estimate the concentration of the  
163 compounds measured by the  $\text{NH}_4^+$ -Orbitrap according to the following equation:

$$164 \quad [prod]_{Orbi\_LTOF/PTR3} = c_{Orbi\_LTOF/PTR3} \times \frac{[(prod)-\text{NH}_4^+] + [(prod)-\text{H}^+]}{\Sigma[\text{Amine}]} \quad (3)$$

165 where  $c$  is the calibration factor, obtained from the correlation analysis. Finally, a temperature-  
166 dependent sampling-line loss correction factor was applied (Simon et al., 2020).

### 167 **2.3 Product analysis by CI-( $\text{NO}_3^-$ )-API-LTOF**

168 Detection of  $\text{RO}_2$  radicals and closed-shell products was also performed by the CI-( $\text{NO}_3^-$ )-LTOF  
169 which has been described elsewhere (Jokinen et al., 2012; Kurten et al., 2014). Therefore, only  
170 relevant details for this study are provided here. The  $\text{NO}_3^-$ -LTOF used in this study had a mass  
171 resolving power of  $m/\Delta m$  12,000 and detected OOMs (mass 300-650 Da) as clusters ions with  
172  $(\text{HNO}_3)_n(\text{NO}_3^-)$  anions, with  $n = 0-2$ . The primary ions were produced by a corona discharge needle  
173 exposed to a sheath gas enriched by  $\text{HNO}_3$ . Laminar flow diffusional loss was assumed in the 30 cm  
174 sampling line. A core-sampling technique was applied (Knopf et al., 2015), which drew a core flow of  
175 5.1 slpm from the center of a 30 slpm total flow. This setup reduced the sampling loss rate of HOMs to  
176 less than 30% (Simon et al., 2020). The data were processed using Tofware (Version 3.2, Aerodyne  
177 Inc., USA) and MATLAB R2019b (MathWorks, Inc., USA). In addition, background signals, mass-  
178 dependent transmission efficiency (Heinritzi et al., 2016), and sampling losses (Simon et al., 2020)  
179 were determined and corrections were applied. The  $\text{NO}_3^-$ -LTOF was directly calibrated using sulfuric  
180 acid (Kurten et al., 2012). A calibration factor  $C$  was determined to be  $\sim 4.13 \times 10^{10}$  molecules  $\text{cm}^{-3}$   
181 during CLOUD14 (Caudillo et al., 2021).

### 182 **2.4 Product analysis by PTR3-TOF**

183 The PTR3-TOF ionizes organic compounds by proton transfer where  $\text{H}_3\text{O}^+$  ions were produced by a  
184 corona discharge using humidified nitrogen (Breitenlechner et al., 2017). To reduce sample losses, a 2  
185 slpm was drawn from a 10 slpm laminar flow through a critical orifice into the tripole where the ion-  
186 molecule reactions occur. The pressure in this region was maintained at  $\sim 80$  mbar. The distribution of  
187 primary ions and sample molecules can be adjusted by a tunable radio frequency signal applied to the  
188 tripole rods.

189 During the CLOUD14 experiments, the collision energy was controlled between 62 and 72 Td to  
190 reduce the methods humidity dependence which may complicate the detection of organic compounds.  
191 The PTR3-TOF was calibrated using a gas standard mixture containing 1 ppm of 3-hexanone,  
192 heptanone, and  $\alpha$ -pinene in nitrogen. The concentration of oxygenated products was estimated using  
193 the sensitivity of 3-hexanone as lower-limit values due to possible fragmentation. All data were  
194 analyzed using TOF-Tracer software running on Julia 0.6 (<https://github.com/lukasfischer83/TOF-Tracer>)  
195 and were further corrected for the duty cycle transmission of TOF and temperature dependent  
196 sampling line losses (Stolzenburg et al., 2018).



## 197 2.5 Product analysis by $\Gamma$ -FIGAERO-CIMS

198 The  $\Gamma$ -FIGAERO-CIMS was capable of characterizing both gas and particle phases (Lopez-Hilfiker et  
199 al., 2014). In the gas-phase mode, gases were directly sampled into a 100-mbar turbulent ion-molecule  
200 reactor, while particles were collected onto a polytetrafluoroethylene (PTFE) filter through a separate  
201 dedicated sampling port. Analytes were then ionized with  $\Gamma$  chemical ionization and extracted into a  
202 TOF mass analyzer (Wang et al., 2020). In this study, only gas phase data are reported.

203 Iodide ions ( $\Gamma$ ) were used as the reagent ions and formed by passing a 1.0 slpm flow of ultrahigh  
204 purity  $\text{N}_2$  over a diffusion tube filled with methyl iodide ( $\text{CH}_3\text{I}$ ), and then through a  $^{210}\text{Po}$  radioactive  
205 source. In the sampling mode, the reagent ion flow was mixed with a sample flow in the IMR at  $\sim 150$   
206 mbar. Coaxial core sampling was used to minimize the vapor wall loss in the sampling line. The total  
207 flow was kept at 18.0 slpm and the core flow at 4.5 slpm; the instrument sampled at the center of the  
208 core flow with a flow rate of 1.6 slpm. The gas-phase background signal was determined by routinely  
209 introducing zero air directly into the inlet. Data were analyzed using Tofware (2.5.11\_FIGAERO  
210 version; Aerodyne Inc., USA) giving 10 s average mass spectra. The ion signal was normalized by the  
211 sum of reagent ion signals (i.e.,  $m/Q$  127:  $\Gamma$  and 145:  $\text{H}_2\text{OI}^-$ ).

## 212 2.6 Volatility of OOMs

213 It is challenging to directly measure the vapor pressure of individual OOMs due to the difficulty to  
214 acquire authentic standards. To overcome experimental challenges, model calculations have been  
215 developed to estimate the vapor pressure using, for example, structure-based estimations and formula-  
216 based estimations (Pankow and Asher, 2008). Volatility basis set (VBS), a categorization framework  
217 based on quantifiable organic property (i.e., volatility) has been established and is frequently used to  
218 characterize oxidation chemistry (Donahue et al., 2011; Li et al., 2016). The VBS parameterization is  
219 useful for classifying the wide range of OOMs into multiple volatility groups, including extremely low  
220 volatility organic compounds (ELVOC) and low volatility organic compounds (LVOC) based on their  
221 effective saturation concentration ( $C^*$ ) in the unit of  $\mu\text{g m}^{-3}$  (Bianchi et al., 2019). In this study, we  
222 applied the VBS parameterization optimized by Li et al (Li et al., 2016; Isaacman-Vanwertz and  
223 Aumont, 2021).

$$224 \quad \log_{10} C^*(298\text{K}) = (n_C^0 - n_C) b_C - n_O b_O - 2 \frac{n_C n_O}{(n_C + n_O)} b_{CO} - n_N b_N - n_S b_S \quad (4)$$

225 where  $n_C$ ,  $n_O$ ,  $n_N$ , and  $n_S$  was the number of carbon, oxygen, nitrogen, and sulfur atoms of the  
226 specific molecule, separately;  $n_C^0$  was the reference carbon number;  $b_C$ ,  $b_O$ ,  $b_N$ , and  $b_S$  was the  
227 contribution of each atom to  $\log_{10} C^*$ , respectively;  $b_{CO}$  was the carbon-oxygen nonideality (Donahue  
228 et al., 2011). Values of  $b$  coefficient can be found in Li et al. (Li et al., 2016). The formula used to  
229 estimate the vapor pressure was amended to convert all  $\text{NO}_3$  groups into OH groups to reduce the bias  
230 from the compounds containing nitrates (Daumit et al., 2013; Isaacman-Vanwertz and Aumont, 2021).





231 Due to the different temperatures in the CLOUD14 experiments, we adjusted  $C^*(298K)$  to the  
232 measured experimental temperature in equations (5) and (6):

$$233 \quad \log_{10}C^*(T) = \log_{10}C^*(298K) + \frac{\Delta H_{vap}}{R \ln(10)} \times \left(\frac{1}{298} - \frac{1}{T}\right) \quad (5)$$

$$234 \quad \Delta H_{vap}(kJ \text{ mol}^{-1}) = -11 \cdot \log_{10}C^*(298K) + 129 \quad (6)$$

235 where  $T$  was the temperature in Kelvin,  $C^*(298K)$  was the saturation vapor concentration at 298 K,  
236  $\Delta H_{vap}$  was the evaporation enthalpy and  $R$  was the gas constant ( $8.3134 \text{ J K}^{-1} \text{ mol}^{-1}$ ). The potential  
237 presence of isomers may result in uncertainty in this method since the only input is the compound's  
238 molecular formula.

239 In this study, all oxidation products were grouped into six volatility regimes; ultralow-volatility  
240 (ULVOCs,  $C^* < 10^{-8.5} \mu\text{g m}^{-3}$ ), extremely low volatility (ELVOCs,  $10^{-8.5} < C^* < 10^{-4.5} \mu\text{g m}^{-3}$ ), low-  
241 volatility (LVOCs,  $10^{-4.5} < C^* < 10^{-0.5} \mu\text{g m}^{-3}$ ), semi-volatile (SVOCs,  $10^{-0.5} < C^* < 10^{2.5} \mu\text{g m}^{-3}$ ),  
242 intermediate-volatility organic compounds (IVOC,  $10^{2.5} < C^* < 10^{6.5} \mu\text{g m}^{-3}$ ), and VOC ( $10^{6.5} < C^* \mu\text{g}$   
243  $\text{m}^{-3}$ ) based on VBS.

## 244 3 Results and Discussions

### 245 3.1 Characterization of $\text{NH}_4^+$ -Orbitrap

246 First, the ability of the higher mass resolving power of the Orbitrap for separating overlapping mass  
247 spectral peaks was compared to other TOF mass analyzers (Riva et al., 2019a; Riva et al., 2020). The  
248 identification and quantification of peaks with low intensity were most affected by overlapping  
249 signals, therefore, the relative intensities of neighboring peaks should also be considered when  
250 estimating their ease of separation.

251 The mass resolving power was defined as

$$252 \quad \text{mass resolving power} = m / \Delta m \quad (7)$$

253 where  $m$  was the mass-to-charge ratio of the analyte ion, and  $\Delta m$  was the full width at half maximum  
254 (FWHM). Higher mass resolving power allows unambiguous mass spectral peak assignment. For a  
255 pair of overlapping peaks of equal intensity, the distance between their respective peak center, referred  
256 to hereafter simply as peak distance,  $dm$ , needed to be greater than approximately 0.8 of the FWHM of  
257 the overlapping peaks, such that they could be reasonably deconvolved as shown in Fig. S2.

258 Depending on their experience, individuals may be able to visually identify the presence of  
259 overlapping peaks at lower or higher  $dm$  values. We arbitrarily defined the minimum  $dm$  (normalized  
260 to that of FWHM, or  $\Delta m$ ) as the value at which the observed spectrum (“Combined” trace in Fig. 1  
261 and S2) had a local minimum between the centers of the overlapping peaks (i.e., there was a “dip” in  
262 the observed signal between ion peaks). The minimum  $dm$  value increased with the intensity ratio of  
263 overlapping peaks, ranging roughly from 0.85 (for equally intense peaks) to 1.43 (for peaks differing  
264 one order of magnitude in their respective intensities), as shown in Fig. 1. In practice, noise and the





265 presence of additional neighboring peaks would further complicate peak deconvolution. For  
266 simplicity, we used a normalized  $dm$  of 1 (i.e.,  $dm = \Delta m$ ) as a threshold for unambiguous  
267 deconvolution of neighboring peaks.

268 Figure 2 shows the histogram of the distances between neighboring peaks normalized against the  
269 FWHM for the Orbitrap mass analyzer and a TOF analyzer having a mass resolving power of 10,000.  
270 In each histogram, one count indicated that an ion had at least one neighboring ion with a relative  
271 intensity of 20%, 50%, or 100% (with a higher relative intensity threshold value being less selective).  
272 Neighboring ions separated by distances exceeding 2 times the FWHM were considered well-  
273 separated. For ions with multiple neighboring peaks within the 2 x FWHM separation distance  
274 window, the distance to the first neighboring peak that satisfied the aforementioned relative intensity  
275 threshold was reported. Overall,  $\text{NH}_4^+$ -Orbitrap can separate most of the observed ions (> 99%), while  
276 the  $\text{Cl}-(\text{NO}_3^-)$ -TOF, depending on the relative intensity threshold set, can separate only 32% to 46% of  
277 all the ions by at least 1 FWHM.

### 278 3.2 Characterization of OVOC by four instruments

279 Illustrated in Fig. 3 are Kendrick mass defect plots of OOMs measured by  $\text{Cl}-(\text{NH}_4^+)$ -Orbitrap,  $\text{Cl}-$   
280  $(\text{NO}_3^-)$ -LTOF, PTR3-TOF, and  $\Gamma$ -FIGAERO-CIMS, identifying species of 484, 252, 145, and 67,  
281 respectively. The  $\text{NH}_4^+$ -Orbitrap detected the widest range of products, including HOMs and the less  
282 oxidized species (i.e.,  $\text{O} < 6$ ). Out of the 484 compounds, 5% were amines. The number of O atoms in  
283 OOMs varied from 1 to 11 in monomers ( $\text{C}_2$ - $\text{C}_{10}$ ) and from 2 to 16 for dimeric products ( $\text{C}_{14}$ - $\text{C}_{20}$ ), with  
284 an average elemental oxygen-to-carbon ratio (O:C) of  $0.4 \pm 0.2$ . As expected, the  $\text{NO}_3^-$ -LTOF  
285 exhibited a very good sensitivity towards HOMs, with the highest O:C of  $0.7 \pm 0.3$ . The PTR3-TOF  
286 mainly detected compounds below  $m/Q$  300 Th with an average O:C of  $0.5 \pm 0.3$ . However, the  
287 PTR3-TOF was optimized (i.e., lowering E/N value) to achieve sensitive measurements of ammonia  
288 and amines, impacting its capability to detect OOMs. Gas-phase concentrations of OOMs were too  
289 low to be efficiently detected in real-time via the gas-phase sampling port of the  $\Gamma$ -FIGAERO-CIMS.  
290 As a result, fewer monomers of  $\text{C}_{8-10}$  and dimers of  $\text{C}_{19-20}$  were observed, with an average O:C of  $0.5 \pm$   
291  $0.2$ .

### 292 3.3 Instrumental comparisons: correlations

293 Due to differences in selectivity and sensitivity of the analytical methods toward OOMs, only a  
294 fraction (~22%) of the identified species can be compared among two or more mass spectrometers. To  
295 identify how  $\text{NH}_4^+$ -Orbitrap performed compared to the other mass spectrometers, a correlation  
296 analysis including all co-detected ions was compiled. The experimental conditions of the runs used for  
297 performing this analysis are summarized in Table S1. The data set covered a variety of conditions,  
298 such as different concentrations of  $\alpha$ -pinene,  $\text{NO}_x$ ,  $\text{SO}_2$ , and CO, as well as RH. A Pearson correlation  
299 coefficient  $R^2$  was calculated, using the time series of OOMs having the same elemental composition  
300 measured by the different mass spectrometers. Figure 4 displays the correlation coefficient of detected  
301 compounds, with marker size scaled by  $R^2$ . The  $\text{NH}_4^+$ -Orbitrap showed  $R^2 > 0.80$  for ~30% of the



302 compounds co-detected with the  $\text{NO}_3^-$ -LTOF. In addition, it demonstrated high correlations with  
303 PTR3-TOF including 89 species having a  $R^2 > 0.50$ .  $\Gamma$ -FIGAERO-CIMS showed  $R^2 > 0.90$  for certain  
304 families of compounds, including  $\text{C}_{10}\text{H}_{15}\text{O}_{5-7}\text{N}$  and  $\text{C}_{20}\text{H}_{31}\text{O}_{7,9}\text{N}$ . By comparing the coverage regions  
305 of the instruments across multiple experimental conditions, the  $\text{NH}_4^+$ -Orbitrap was capable of covering  
306 the widest range of compounds and showed an overall good agreement with other mass spectrometers.

### 307 **3.4 Instrumental comparisons: concentration estimates**

308 Concentrations of the identified compounds were estimated for  $\text{NH}_4^+$ -Orbitrap, as described in section  
309 2.2. The sensitivity of  $\text{NH}_4^+$ -Orbitrap was constrained using semi-quantitative information from the  
310 other instruments. For instance, concentrations of the most abundant  $\text{C}_{10}$ -monomers (i.e.,  $\text{C}_{10}\text{H}_{14/16}\text{O}_n$ )  
311 were estimated using different calibration factors (Fig. 5), which were measured during steady-state  
312 conditions (i.e., Run 2211 with  $[\text{O}_3] = 100$  ppbv and  $[\alpha\text{-pinene}] = 2$  ppbv,  $\text{RH} = 10\%$ ). Using  
313 calibration factors obtained from two independent correlation analyses (i.e., using the PTR3-TOF and  
314 the  $\text{NO}_3^-$ -LTOF), concentrations of  $\text{C}_{10}$ -monomers measured by  $\text{NH}_4^+$ -Orbitrap were within a factor of  
315 2, showing a good agreement between the different instruments and underlining the robustness of the  
316 methodology. As previously reported, the Orbitrap had a non-linear response to compounds present at  
317 extremely low concentrations, which was independent of the sample composition, instrumental setup,  
318 or the reagent ion (Riva et al., 2020; Cai et al., 2022). A similar evaluation was performed for the  
319  $\text{NH}_4^+$ -Orbitrap by comparing the measured versus the theoretical isotopic intensities. As shown in Fig.  
320 S3, the  $\text{NH}_4^+$ -Orbitrap had a linear response for ion intensity greater than  $\sim 5 \times 10^3$  cps, which  
321 corresponded to a limit of quantification (LoQ, corresponding to the lowest normalized signal  
322 observed within the linear range) of  $\sim 5 \times 10^5$  molecules  $\text{cm}^{-3}$  for OOMs, estimated using the  
323 calibration factor derived from  $\text{NO}_3^-$ -LTOF; which is consistent with a previous study (Riva et al.,  
324 2020).

325 Figure 6 presents the concentrations of all OVOCs measured by the  $\text{NH}_4^+$ -Orbitrap determined by  
326 applying two different calibration factors. Compared to other mass spectrometers, the  $\text{NH}_4^+$ -Orbitrap  
327 captured the largest fraction of the reacted carbon. Of the most abundant oxidation products,  
328 pinonaldehyde (i.e.,  $\text{C}_{10}\text{H}_{16}\text{O}_2$ ) was not efficiently detected by  $\text{NO}_3^-$ -LTOF, which is consistent with  
329 the higher selectivity of the  $\text{NO}_3^-$  reagent ion. To further illustrate the selectivity of the different  
330 reagent ions, Fig. 7 offers a summary of the performance of each mass spectrometer in detecting  
331 monomeric compounds, such as  $\text{C}_{10}\text{H}_{16}\text{O}_n$ . The y-axis is arbitrary and represents a qualitative  
332 characterization of the oxygen content when compounds were detected by different CI schemes.  
333 Similar to previous results, the  $\Gamma$ -FIGAERO-CIMS detected OOMs with  $n_{\text{O}} > 3$ , but was not optimal  
334 for the detection of monomers with  $n_{\text{O}} > 7$  (Riva et al., 2019b). The  $\text{NO}_3^-$ -LTOF was mainly selective  
335 towards HOMs with  $n_{\text{O}} > 6$  (Riva et al., 2019b). The PTR3-TOF had limited capabilities in detecting  
336 OOMs with  $n_{\text{O}} > 5$  due to the optimization of the instrument to obtain a very sensitive measurement of  
337 ammonia. Previously, the amine-CI demonstrated promise for the detection of OOMs, but was limited  
338 to applications with comparatively clean conditions due to considerable depletion of the reagent ion  
339 and the presence of overlapping peaks (Berndt et al., 2017; Berndt et al., 2018b; Riva et al., 2019b).



340 While showing a similar OOMs detection range to amine-CI,  $\text{NH}_4^+$ -CI in tandem with the greater mass  
341 resolving power of the Orbitrap mass analyzer provided a linear response to higher loading. As shown  
342 in Fig. S4, background peaks were not affected by atmospherically relevant concentrations of  $\text{O}_3$  and  
343  $\alpha$ -pinene. Overall, the  $\text{NH}_4^+$ -Orbitrap appears to have the potential for providing a more reliable  
344 identification/quantification of OOMs produced from VOC oxidation compared to other existing mass  
345 spectrometry techniques.

### 346 3.5 Volatility distribution by four instruments

347 Figure 8 shows the distribution of oxidation products measured by four MS instruments according to  
348 their saturation vapor concentrations ( $\log_{10}C_{\text{sat}}$ ) estimated using the modified Li et al. approach (Li et  
349 al., 2016; Isaacman-Vanwertz and Aumont, 2021). OOMs were grouped into six volatility regimes  
350 based on a volatility basis set (VBS): ultra-low volatility (ULVOCs); extremely low volatility  
351 (ELVOCs); low-volatility (LVOCs); semi-volatile (SVOCs); intermediate volatility organic  
352 compounds (IVOC); and VOC. ULVOCs and ELVOCs initiate cluster growth and form new particles.  
353 The total signal in each volatility bin represented the sum of the signal intensity of OOMs within the  
354 volatility range. The mean contributions of these compound regimes are shown in the VBS pie charts.  
355 The ULVOC, ELVOC, and LVOC regimes were well captured by  $\text{NH}_4^+$ -Orbitrap and  $\text{NO}_3^-$ -LTOF.  
356 The PTR3-TOF only characterized the SVOC and IVOC regime (along with VOCs). IVOC and VOC  
357 regimes in the PTR3-TOF and  $\text{NH}_4^+$ -Orbitrap were generally less oxygenated VOCs (i.e.,  $n_{\text{O}} < 5$ ).  
358 IVOC comprised the biggest mass contributions for the  $\text{NH}_4^+$ -Orbitrap, and LVOC dominated in the  
359  $\text{NO}_3^-$ -LTOF. Hence, the detection of the  $\text{NH}_4^+$ -Orbitrap covered the widest range of volatilities,  
360 clearly highlighting the benefit of using this technique for the formation and fate of OOMs. In the past,  
361 reagent switching has not been practical, and users would run multiple mass spectrometer systems in  
362 parallel or use a Multi-scheme chemical IONization inlet (MION) with only one mass spectrometer to  
363 obtain the fullest possible mass spectrum (Rissanen et al., 2019; Huang et al., 2021). With  $\text{NH}_4^+$ -  
364 Orbitrap it is now possible to cover the entire range of compounds which was not the case with most  
365 CI techniques.

### 366 3.6 RH dependance of $\text{NH}_4^+$ -Orbitrap

367 The sensitivity of the reagent-adduct ionization has been reported to be affected by the presence of  
368 water vapor for a variety of reagent ions (Lee et al., 2014; Breitenlechner et al., 2017). The impact of  
369 RH on the detection of OOMs by the  $\text{NH}_4^+$ -Orbitrap was also studied. While the concentrations of gas  
370 phase precursor and oxidant remained constant the RH was raised from 10% to 80%. During this  
371 increase the signal of organic vapor behaved inconsistently, presumably due to the increased  
372 partitioning of SVOCs to the particle phase under an otherwise constant gas-phase production rate  
373 (Surdu et al., 2023) and an increase in the condensation sink (Fig. S5). As shown in Fig. 9, the  $\text{NH}_4^+$ -  
374 Orbitrap demonstrated an RH dependence. For instance, the signal of less oxygenated molecules (i.e.,  
375  $n_{\text{O}} < 5$ ) increased with increasing RH, especially compounds with  $n_{\text{C}} = 8$ ; while the signal of highly  
376 oxygenated molecules (i.e.,  $n_{\text{O}} > 10$ ) decreased as a function of RH. The average behavior of all  $\text{C}_{8-10}$   
377 monomers and  $\text{C}_{18-20}$  dimers was summarized and compared between four instruments (Fig. S6). The



378 other three mass spectrometers also showed obvious RH dependence. The evolution of the signal  
379 intensity of the ions measured by the  $\text{NH}_4^+$ -Orbitrap with changing RH may be explained by multiple  
380 reasons, such as water affecting the ionization efficiency or altering the physicochemical processes of  
381 the gas phase chemistry.

382 First, the efficiency of a particular compound partly relied on whether water vapor competes with  
383 the ammonium ion, lowering the sensitivity, or whether it acted as a third body to stabilize the  
384 ammonium-organic analyte cluster by removing extra energy from the collision, raising the sensitivity  
385 (Lee et al., 2014).  $\text{NH}_4^+$  primary ions can cluster with water molecules when humidity increased,  
386 thereby reducing the clustering of the  $\text{NH}_4^+$  with organic analytes (Breitenlechner et al., 2017).  
387 However, the formed  $\text{NH}_4^+\text{X}_n$  (X being  $\text{NH}_3$  or  $\text{H}_2\text{O}$ ;  $n = 1,2$ ) clusters might also act as reagent ions  
388 and ionized OOMs through ligand switching reactions, which were expected to be fast and thus  
389 improve the charging efficiency (Hansel et al., 2018). Compared to previous  $\text{NH}_4^+$ -CIMS, the  $\text{NH}_4^+\text{X}_n$   
390 reagent ions were expected to be larger due to the absence of the field in the ion-molecular-reaction  
391 zone in Orbitrap, resulting in greater ligand exchanging and increasing the sensitivity for the less  
392 oxygenated species (Canaval et al., 2019). For RH-independent compounds, this may be due to the  
393 existence of very stable complexes with  $\text{NH}_4^+$  reagent ion, or sufficient internal vibrational modes to  
394 disperse extra energy from the collision (Lee et al., 2014). The highly oxygenated dimers in the  
395 category of ULVOCs and ELVOCs which largely partition to the particle phase regardless of the  
396 presence of water might indicate that water may also affect the physicochemical processes (i.e.,  
397 multiphase chemistry, partitioning, etc.), in this case possibly causing the decomposition of highly  
398 oxygenated molecules in the particle phase to create less and moderately oxygenated products, e.g.,  
399  $\text{C}_8\text{H}_{12}\text{O}_{1.5}$  (up to a 30-fold increase in the gas phase) (Pospisilova et al., 2020), and/or leading to an  
400 increase in the driving force of gas-particle partitioning of highly oxygenated species (Surdu et al.,  
401 2023). Finally, while water vapor could affect the gas-phase chemistry through water reactions with  
402 the Criegee intermediates (CIs),  $\text{HO}_2$  chemistry, OH radical concentration, no clear evidence has been  
403 identified as earlier discussed by Surdu et al (2023).

#### 404 **4 Summary**

405 In conclusion, this study presented an intercomparison between CI-( $\text{NH}_4^+$ )-Orbitrap, CI-( $\text{NO}_3^-$ )-LTOF,  
406 PTR3-TOF, and I-FIGAERO-CIMS based on the identification and quantification of OOMs formed  
407 from the ozonolysis of  $\alpha$ -pinene under various environmental conditions. We used for the first time,  
408  $\text{NH}_4^+$  adduct ions with the Orbitrap mass spectrometer to measure the oxygenated species.  $\text{NH}_4^+$ -  
409 Orbitrap was a promising CIMS technique for a comprehensive measurement of the whole product  
410 distribution and provides a more complete understanding of the molecular composition and volatility  
411 of OOMs. This allows  $\text{NH}_4^+$ -Orbitrap to better monitor the evolution of organic compounds, which  
412 can be beneficial for air quality, pollutant transport, and climate models. However, it remains  
413 challenging to obtain an accurate quantification of the trace gaseous substances at pptv levels. It is  
414 worth expecting that  $\text{NH}_4^+$ -Orbitrap can be not only useful for laboratory-based studies but also to  
415 field observations, to provide a deeper understanding of atmospheric oxidation processes.



416 **Conflicts of interest**

417 At least one of the (co-)authors is a member of the editorial board of Atmospheric Measurement  
418 Techniques

419 **Acknowledgements**

420 We thank the European Organization for Nuclear Research (CERN) for supporting CLOUD with  
421 important technical and financial resources. We thank the Orbitool team for developing the tools to  
422 analyze mass spectra. This work was financially supported by the French National program LEFE  
423 (Les Enveloppes Fluides et l'Environnement), the European Research Council (ERC-StG MAARvEL;  
424 no. 852161), the European Union's Horizon 2020 research and innovation programme (Marie  
425 Skłodowska-Curie grant agreement no. 764991 and 701647), the Swiss National Science Foundation  
426 (no. 200021\_169090, 200020\_172602, 20FI20\_172622, and 206021\_198140), the US National  
427 Science Foundation (NSF\_AGS\_1801280, NSF\_AGC\_1801574, NSF\_AGS\_1801897,  
428 NSF\_AGS\_2132089), and the German Federal Ministry of Education and Research (CLOUD-16  
429 01LK1601A). D.D.L. thanks the China Scholarship Council of P. R. China for the Ph.D. grant.  
430 M.Y.W. acknowledges financial support from the Schmidt Science Fellows Program by Schmidt  
431 Futures, in partnership with the Rhodes Trust.

432 **Author Contributions**

433 D.D.L., D.Y.W., L.C., W.S., M.Y.W., S.T., G.M., M.S., E.E., X.D.G., L.G.-C., M.G., J.P., B.R., B.S.,  
434 P.R., S.P., A.H., J.C., J.K., N.M.D., C.G., I.E.-H., and M.R. prepared the CLOUD facility or  
435 measuring instruments. D.D.L., D.Y.W., L.C., W.S., M.Y.W., S.T., G.M., M.S., E.E., X.D.G., L.G.-  
436 C., M.G., J.P., B.R., B.S., J.K., and M.R. collected the CLOUD data. D.D.L., D.Y.W., L.C., W.S.,  
437 M.Y.W., G.M., and M.R. analysed the data. D.D.L., D.Y.W., M.Y.W., N.M.D., C.G., I.E.-H., and  
438 M.R. wrote the manuscript and contributed to the scientific discussion. All authors discussed the  
439 results and commented on the paper.

440 **References**

- 441 Berndt, T., Herrmann, H., and Kurten, T.: Direct Probing of Criegee Intermediates from Gas-Phase  
442 Ozonolysis Using Chemical Ionization Mass Spectrometry, *J. Am. Chem. Soc.*, 139, 13387-13392,  
443 10.1021/jacs.7b05849, 2017.
- 444 Berndt, T., Mentler, B., Scholz, W., Fischer, L., Herrmann, H., Kulmala, M., and Hansel, A.: Accretion  
445 Product Formation from Ozonolysis and OH Radical Reaction of alpha-Pinene: Mechanistic Insight  
446 and the Influence of Isoprene and Ethylene, *Environ. Sci. Technol.*, 52, 11069-11077,  
447 10.1021/acs.est.8b02210, 2018a.
- 448 Berndt, T., Scholz, W., Mentler, B., Fischer, L., Herrmann, H., Kulmala, M., and Hansel, A.: Accretion  
449 Product Formation from Self- and Cross-Reactions of RO<sub>2</sub> Radicals in the Atmosphere, *Angew.  
450 Chem. Int. Ed.*, 57, 3820-3824, 10.1002/anie.201710989, 2018b.
- 451 Berndt, T., Richters, S., Kaethner, R., Voigtlander, J., Stratmann, F., Sipila, M., Kulmala, M., and  
452 Herrmann, H.: Gas-Phase Ozonolysis of Cycloalkenes: Formation of Highly Oxidized RO<sub>2</sub> Radicals  
453 and Their Reactions with NO, NO<sub>2</sub>, SO<sub>2</sub>, and Other RO<sub>2</sub> Radicals, *J. Phys. Chem. A*, 119, 10336-  
454 10348, 10.1021/acs.jpca.5b07295, 2015.



- 455 Bianchi, F., Kurten, T., Riva, M., Mohr, C., Rissanen, M. P., Roldin, P., Berndt, T., Crouse, J. D.,  
456 Wennberg, P. O., Mentel, T. F., Wildt, J., Junninen, H., Jokinen, T., Kulmala, M., Worsnop, D. R.,  
457 Thornton, J. A., Donahue, N., Kjaergaard, H. G., and Ehn, M.: Highly Oxygenated Organic  
458 Molecules (HOM) from Gas-Phase Autoxidation Involving Peroxy Radicals: A Key Contributor to  
459 Atmospheric Aerosol, *Chem. Rev.*, 119, 3472-3509, 10.1021/acs.chemrev.8b00395, 2019.
- 460 Bianchi, F., Tröstl, J., Junninen, H., Frege, C., Henne, S., Hoyle, C. R., Molteni, U., Herrmann, E.,  
461 Adamov, A., Bukowiecki, N., Chen, X., Duplissy, J., Gysel, M., Hutterli, M., Kangasluoma, J.,  
462 Kontkanen, J., Kürten, A., Manninen, H. E., Münch, S., Peräkylä, O., Petäjä, T., Rondo, L.,  
463 Williamson, C., Weingartner, E., Curtius, J., Worsnop, D. R., Kulmala, M., Dommen, J., and  
464 Baltensperger, U.: New particle formation in the free troposphere: A question of chemistry and  
465 timing, *Science*, 352, 1109-1112, 10.1126/science.aad5456, 2016.
- 466 Breitenlechner, M., Fischer, L., Hainer, M., Heinritzi, M., Curtius, J., and Hansel, A.: PTR3: An  
467 Instrument for Studying the Lifecycle of Reactive Organic Carbon in the Atmosphere, *Anal. Chem.*,  
468 89, 5824-5831, 10.1021/acs.analchem.6b05110, 2017.
- 469 Cai, R., Huang, W., Meder, M., Bourgain, F., Aizikov, K., Riva, M., Bianchi, F., and Ehn, M.: Improving  
470 the Sensitivity of Fourier Transform Mass Spectrometer (Orbitrap) for Online Measurements of  
471 Atmospheric Vapors, *Anal. Chem.*, 94, 15746-15753, 10.1021/acs.analchem.2c03403, 2022.
- 472 Cai, R., Li, Y., Clément, Y., Li, D., Dubois, C., Fabre, M., Besson, L., Perrier, S., George, C., Ehn, M.,  
473 Huang, C., Yi, P., Ma, Y., and Riva, M.: Orbitool: a software tool for analyzing online Orbitrap mass  
474 spectrometry data, *Atmos. Meas. Tech.*, 14, 2377-2387, 10.5194/amt-14-2377-2021, 2021.
- 475 Canaval, E., Hyttinen, N., Schmidbauer, B., Fischer, L., and Hansel, A.:  $\text{NH}_4^+$  Association and Proton  
476 Transfer Reactions With a Series of Organic Molecules, *Front. Chem.*, 7, 10.3389/fchem.2019.00191,  
477 2019.
- 478 Caudillo, L., Rörup, B., Heinritzi, M., Marie, G., Simon, M., Wagner, A. C., Müller, T., Granzin, M.,  
479 Amorim, A., Ataei, F., Baalbaki, R., Bertozzi, B., Brasseur, Z., Chiu, R., Chu, B., Dada, L., Duplissy,  
480 J., Finkenzeller, H., Gonzalez Carracedo, L., He, X. C., Hofbauer, V., Kong, W., Lamkaddam, H.,  
481 Lee, C. P., Lopez, B., Mahfouz, N. G. A., Makhmutov, V., Manninen, H. E., Marten, R., Massabò,  
482 D., Mauldin, R. L., Mentler, B., Molteni, U., Onnela, A., Pfeifer, J., Philippov, M., Piedehierro, A.  
483 A., Schervish, M., Scholz, W., Schulze, B., Shen, J., Stolzenburg, D., Stozhkov, Y., Surdu, M.,  
484 Tauber, C., Tham, Y. J., Tian, P., Tomé, A., Vogt, S., Wang, M., Wang, D. S., Weber, S. K., Welti,  
485 A., Yonghong, W., Yusheng, W., Zauner-Wieczorek, M., Baltensperger, U., El Haddad, I., Flagan,  
486 R. C., Hansel, A., Höhler, K., Kirkby, J., Kulmala, M., Lehtipalo, K., Möhler, O., Saathoff, H.,  
487 Volkamer, R., Winkler, P. M., Donahue, N. M., Kürten, A., and Curtius, J.: Chemical composition  
488 of nanoparticles from  $\alpha$ -pinene nucleation and the influence of isoprene and relative humidity at low  
489 temperature, *Atmos. Chem. Phys.*, 21, 17099-17114, 10.5194/acp-21-17099-2021, 2021.
- 490 Crouse, J. D., Nielsen, L. B., Jørgensen, S., Kjaergaard, H. G., and Wennberg, P. O.: Autoxidation of  
491 Organic Compounds in the Atmosphere, *J. Phys. Chem. Lett.*, 4, 3513-3520, 10.1021/jz4019207,  
492 2013.
- 493 Daumit, K. E., Kessler, S. H., and Kroll, J. H.: Average chemical properties and potential formation  
494 pathways of highly oxidized organic aerosol, *Faraday discussions*, 165, 181-202,  
495 10.1039/c3fd00045a, 2013.





- 496 Donahue, N. M., Epstein, S. A., Pandis, S. N., and Robinson, A. L.: A two-dimensional volatility basis  
497 set: 1. organic-aerosol mixing thermodynamics, *Atmos. Chem. Phys.*, 11, 3303-3318, 10.5194/acp-  
498 11-3303-2011, 2011.
- 499 Ehn, M., Junninen, H., Petäjä, T., Kurtén, T., Kerminen, V. M., Schobesberger, S., Manninen, H. E.,  
500 Ortega, I. K., Vehkamäki, H., Kulmala, M., and Worsnop, D. R.: Composition and temporal behavior  
501 of ambient ions in the boreal forest, *Atmos. Chem. Phys.*, 10, 8513-8530, 10.5194/acp-10-8513-2010,  
502 2010.
- 503 Ehn, M., Thornton, J. A., Kleist, E., Sipila, M., Junninen, H., Pullinen, I., Springer, M., Rubach, F.,  
504 Tillmann, R., Lee, B., Lopez-Hilfiker, F., Andres, S., Acir, I. H., Rissanen, M., Jokinen, T.,  
505 Schobesberger, S., Kangasluoma, J., Kontkanen, J., Nieminen, T., Kurten, T., Nielsen, L. B.,  
506 Jorgensen, S., Kjaergaard, H. G., Canagaratna, M., Maso, M. D., Berndt, T., Petaja, T., Wahner, A.,  
507 Kerminen, V. M., Kulmala, M., Worsnop, D. R., Wildt, J., and Mentel, T. F.: A large source of low-  
508 volatility secondary organic aerosol, *Nature*, 506, 476-479, 10.1038/nature13032, 2014.
- 509 Fan, J., Wang, Y., Rosenfeld, D., and Liu, X.: Review of Aerosol–Cloud Interactions: Mechanisms,  
510 Significance, and Challenges, *J. Atmos. Sci.*, 73, 4221-4252, 10.1175/jas-d-16-0037.1, 2016.
- 511 Glasius, M. and Goldstein, A. H.: Recent Discoveries and Future Challenges in Atmospheric Organic  
512 Chemistry, *Environ. Sci. Technol.*, 50, 2754-2764, 10.1021/acs.est.5b05105, 2016.
- 513 Hallquist, M., Wenger, J. C., Baltensperger, U., Rudich, Y., Simpson, D., Claeys, M., Dommen, J.,  
514 Donahue, N. M., George, C., Goldstein, A. H., Hamilton, J. F., Herrmann, H., Hoffmann, T., Iinuma,  
515 Y., Jang, M., Jenkin, M. E., Jimenez, J. L., Kiendler-Scharr, A., Maenhaut, W., McFiggans, G.,  
516 Mentel, T. F., Monod, A., Prévôt, A. S. H., Seinfeld, J. H., Surratt, J. D., Szmigielski, R., and Wildt,  
517 J.: The formation, properties and impact of secondary organic aerosol: current and emerging issues,  
518 *Atmos. Chem. Phys.*, 9, 5155-5236, 10.5194/acp-9-5155-2009, 2009.
- 519 Hansel, A., Scholz, W., Mentler, B., Fischer, L., and Berndt, T.: Detection of RO<sub>2</sub> radicals and other  
520 products from cyclohexene ozonolysis with NH<sub>4</sub><sup>+</sup> and acetate chemical ionization mass spectrometry,  
521 *Atmospheric Environment*, 186, 248-255, 10.1016/j.atmosenv.2018.04.023, 2018.
- 522 Haywood, J. and Boucher, O.: Estimates of the direct and indirect radiative forcing due to tropospheric  
523 aerosols: A review, *Rev. Geophys.*, 38, 513-543, 2000.
- 524 Heinritzi, M., Simon, M., Steiner, G., Wagner, A. C., Kürten, A., Hansel, A., and Curtius, J.:  
525 Characterization of the mass-dependent transmission efficiency of a CIMS, *Atmos. Meas. Tech.*, 9,  
526 1449-1460, 10.5194/amt-9-1449-2016, 2016.
- 527 Huang, W., Li, H., Sarnela, N., Heikkinen, L., Tham, Y. J., Mikkilä, J., Thomas, S. J., Donahue, N. M.,  
528 Kulmala, M., and Bianchi, F.: Measurement report: Molecular composition and volatility of gaseous  
529 organic compounds in a boreal forest – from volatile organic compounds to highly oxygenated  
530 organic molecules, *Atmos. Chem. Phys.*, 21, 8961-8977, 10.5194/acp-21-8961-2021, 2021.
- 531 Isaacman-VanWertz, G. and Aumont, B.: Impact of organic molecular structure on the estimation of  
532 atmospherically relevant physicochemical parameters, *Atmos. Chem. Phys.*, 21, 6541-6563,  
533 10.5194/acp-21-6541-2021, 2021.
- 534 Jimenez, J. L., Canagaratna, M. R., Donahue, N. M., Prevot, A. S. H., Zhang, Q., Kroll, J. H., DeCarlo,  
535 P. F., Allan, J. D., Coe, H., Ng, N. L., Aiken, A. C., Docherty, K. S., Ulbrich, I. M., Grieshop, A. P.,  
536 Robinson, A. L., Duplissy, J., Smith, J. D., Wilson, K. R., Lanz, V. A., Hueglin, C., Sun, Y. L., Tian,  
537 J., Laaksonen, A., Raatikainen, T., Rautiainen, J., Vaattovaara, P., Ehn, M., Kulmala, M., Tomlinson,  
538 J. M., Collins, D. R., Cubison, M. J., Dunlea, J., Huffman, J. A., Onasch, T. B., Alfarra, M. R.,





- 539 Williams, P. I., Bower, K., Kondo, Y., Schneider, J., Drewnick, F., Borrmann, S., Weimer, S.,  
540 Demerjian, K., Salcedo, D., Cottrell, L., Griffin, R., Takami, A., Miyoshi, T., Hatakeyama, S.,  
541 Shimono, A., Sun, J. Y., Zhang, Y. M., Dzepina, K., Kimmel, J. R., Sueper, D., Jayne, J. T., Herndon,  
542 S. C., Trimborn, A. M., Williams, L. R., Wood, E. C., Middlebrook, A. M., Kolb, C. E., Baltensperger,  
543 U., and Worsnop, D. R.: Evolution of Organic Aerosols in the Atmosphere, *Science*, 326, 1525-1529,  
544 doi:10.1126/science.1180353, 2009.
- 545 Jokinen, T., Sipilä, M., Junninen, H., Ehn, M., Lönn, G., Hakala, J., Petäjä, T., Mauldin, R. L., Kulmala,  
546 M., and Worsnop, D. R.: Atmospheric sulphuric acid and neutral cluster measurements using CI-  
547 API-TOF, *Atmos. Chem. Phys.*, 12, 4117-4125, 10.5194/acp-12-4117-2012, 2012.
- 548 Jokinen, T., Berndt, T., Makkonen, R., Kerminen, V. M., Junninen, H., Paasonen, P., Stratmann, F.,  
549 Herrmann, H., Guenther, A. B., Worsnop, D. R., Kulmala, M., Ehn, M., and Sipilä, M.: Production  
550 of extremely low volatile organic compounds from biogenic emissions: Measured yields and  
551 atmospheric implications, *Proc. Natl. Acad. Sci. U. S. A.*, 112, 7123-7128,  
552 10.1073/pnas.1423977112, 2015.
- 553 Kirkby, J., Curtius, J., Almeida, J., Dunne, E., Duplissy, J., Ehrhart, S., Franchin, A., Gagne, S., Ickes,  
554 L., Kurten, A., Kupc, A., Metzger, A., Riccobono, F., Rondo, L., Schobesberger, S., Tsagkogeorgas,  
555 G., Wimmer, D., Amorim, A., Bianchi, F., Breitenlechner, M., David, A., Dommen, J., Downard, A.,  
556 Ehn, M., Flagan, R. C., Haider, S., Hansel, A., Hauser, D., Jud, W., Junninen, H., Kreissl, F., Kvashin,  
557 A., Laaksonen, A., Lehtipalo, K., Lima, J., Lovejoy, E. R., Makhmutov, V., Mathot, S., Mikkilä, J.,  
558 Minginette, P., Mogo, S., Nieminen, T., Onnela, A., Pereira, P., Petaja, T., Schnitzhofer, R., Seinfeld,  
559 J. H., Sipilä, M., Stozhkov, Y., Stratmann, F., Tome, A., Vanhanen, J., Viisanen, Y., Vrtala, A.,  
560 Wagner, P. E., Walther, H., Weingartner, E., Wex, H., Winkler, P. M., Carslaw, K. S., Worsnop, D.  
561 R., Baltensperger, U., and Kulmala, M.: Role of sulphuric acid, ammonia and galactic cosmic rays  
562 in atmospheric aerosol nucleation, *Nature*, 476, 429-433, 10.1038/nature10343, 2011.
- 563 Kirkby, J., Duplissy, J., Sengupta, K., Frege, C., Gordon, H., Williamson, C., Heinritzi, M., Simon, M.,  
564 Yan, C., Almeida, J., Tröstl, J., Nieminen, T., Ortega, I. K., Wagner, R., Adamov, A., Amorim, A.,  
565 Bernhammer, A.-K., Bianchi, F., Breitenlechner, M., Brilke, S., Chen, X., Craven, J., Dias, A.,  
566 Ehrhart, S., Flagan, R. C., Franchin, A., Fuchs, C., Guida, R., Hakala, J., Hoyle, C. R., Jokinen, T.,  
567 Junninen, H., Kangasluoma, J., Kim, J., Krapf, M., Kürten, A., Laaksonen, A., Lehtipalo, K.,  
568 Makhmutov, V., Mathot, S., Molteni, U., Onnela, A., Peräkylä, O., Piel, F., Petäjä, T., Praplan, A.  
569 P., Pringle, K., Rap, A., Richards, N. A. D., Riipinen, I., Rissanen, M. P., Rondo, L., Sarnela, N.,  
570 Schobesberger, S., Scott, C. E., Seinfeld, J. H., Sipilä, M., Steiner, G., Stozhkov, Y., Stratmann, F.,  
571 Tomé, A., Virtanen, A., Vogel, A. L., Wagner, A. C., Wagner, P. E., Weingartner, E., Wimmer, D.,  
572 Winkler, P. M., Ye, P., Zhang, X., Hansel, A., Dommen, J., Donahue, N. M., Worsnop, D. R.,  
573 Baltensperger, U., Kulmala, M., Carslaw, K. S., and Curtius, J.: Ion-induced nucleation of pure  
574 biogenic particles, *Nature*, 533, 521, 10.1038/nature17953, 2016.
- 575 Knopf, D. A., Poschl, U., and Shiraiwa, M.: Radial diffusion and penetration of gas molecules and  
576 aerosol particles through laminar flow reactors, denuders, and sampling tubes, *Anal. Chem.*, 87,  
577 3746-3754, 10.1021/ac5042395, 2015.
- 578 Kurten, A., Rondo, L., Ehrhart, S., and Curtius, J.: Calibration of a chemical ionization mass  
579 spectrometer for the measurement of gaseous sulfuric acid, *J. Phys. Chem. A*, 116, 6375-6386,  
580 10.1021/jp212123n, 2012.



- 581 Kurten, A., Jokinen, T., Simon, M., Sipila, M., Sarnela, N., Junninen, H., Adamov, A., Almeida, J.,  
582 Amorim, A., Bianchi, F., Breitenlechner, M., Dommen, J., Donahue, N. M., Duplissy, J., Ehrhart, S.,  
583 Flagan, R. C., Franchin, A., Hakala, J., Hansel, A., Heinritzi, M., Hutterli, M., Kangasluoma, J.,  
584 Kirkby, J., Laaksonen, A., Lehtipalo, K., Leiminger, M., Makhmutov, V., Mathot, S., Onnela, A.,  
585 Petaja, T., Praplan, A. P., Riccobono, F., Rissanen, M. P., Rondo, L., Schobesberger, S., Seinfeld, J.  
586 H., Steiner, G., Tome, A., Trostl, J., Winkler, P. M., Williamson, C., Wimmer, D., Ye, P.,  
587 Baltensperger, U., Carslaw, K. S., Kulmala, M., Worsnop, D. R., and Curtius, J.: Neutral molecular  
588 cluster formation of sulfuric acid-dimethylamine observed in real time under atmospheric conditions,  
589 *Proc. Natl. Acad. Sci. U. S. A.*, 111, 15019-15024, 10.1073/pnas.1404853111, 2014.
- 590 Lee, B. H., Lopez-Hilfiker, F. D., Mohr, C., Kurten, T., Worsnop, D. R., and Thornton, J. A.: An iodide-  
591 adduct high-resolution time-of-flight chemical-ionization mass spectrometer: application to  
592 atmospheric inorganic and organic compounds, *Environ. Sci. Technol.*, 48, 6309-6317,  
593 10.1021/es500362a, 2014.
- 594 Li, H., Riva, M., Rantala, P., Heikkinen, L., Daellenbach, K., Krechmer, J. E., Flaud, P.-M., Worsnop,  
595 D., Kulmala, M., Villenave, E., Perraudin, E., Ehn, M., and Bianchi, F.: Terpenes and their oxidation  
596 products in the French Landes forest: insights from Vocus PTR-TOF measurements, *Atmos. Chem.*  
597 *Phys.*, 20, 1941-1959, 10.5194/acp-20-1941-2020, 2020.
- 598 Li, Y., Pöschl, U., and Shiraiwa, M.: Molecular corridors and parameterizations of volatility in the  
599 chemical evolution of organic aerosols, *Atmos. Chem. Phys.*, 16, 3327-3344, 10.5194/acp-16-3327-  
600 2016, 2016.
- 601 Lindinger, W., Hansel, A., and Jordan, A.: On-line monitoring of volatile organic compounds at pptv  
602 levels by means of proton-transfer-reaction mass spectrometry (PTR-MS) medical applications, food  
603 control and environmental research, *Int. J. Mass Spectrom. Ion Process.*, 173, 191-241,  
604 [https://doi.org/10.1016/S0168-1176\(97\)00281-4](https://doi.org/10.1016/S0168-1176(97)00281-4), 1998.
- 605 Lopez-Hilfiker, F. D., Mohr, C., Ehn, M., Rubach, F., Kleist, E., Wildt, J., Mentel, T. F., Lutz, A.,  
606 Hallquist, M., Worsnop, D., and Thornton, J. A.: A novel method for online analysis of gas and  
607 particle composition: description and evaluation of a Filter Inlet for Gases and AEROSols  
608 (FIGAERO), *Atmos. Meas. Tech.*, 7, 983-1001, 10.5194/amt-7-983-2014, 2014.
- 609 Mellouki, A., Wallington, T. J., and Chen, J.: Atmospheric chemistry of oxygenated volatile organic  
610 compounds: impacts on air quality and climate, *Chem. Rev.*, 115, 3984-4014, 10.1021/cr500549n,  
611 2015.
- 612 Pankow, J.F. and Asher W.E. SIMPOL.1: a simple group contribution method for predicting vapor  
613 pressures and enthalpies of vaporization of multifunctional organic compounds. *Atmos. Chem. Phys.*,  
614 8, 2773-2796, 10.5194/acp-8-2773-2008, 2008.
- 615 Pospisilova, V., Lopez-Hilfiker, F. D., Bell, D. M., El Haddad, I., Mohr, C., Huang, W., Heikkinen, L.,  
616 Xiao, M., Dommen, J., Prevot, A. S. H., Baltensperger, U., and Slowik, J. G.: On the fate of  
617 oxygenated organic molecules in atmospheric aerosol particles, *Sci. Adv.*, 6, eaax8922,  
618 doi:10.1126/sciadv.aax8922, 2020.
- 619 Praplan, A. P., Schobesberger, S., Bianchi, F., Rissanen, M. P., Ehn, M., Jokinen, T., Junninen, H.,  
620 Adamov, A., Amorim, A., Dommen, J., Duplissy, J., Hakala, J., Hansel, A., Heinritzi, M.,  
621 Kangasluoma, J., Kirkby, J., Krapf, M., Kürten, A., Lehtipalo, K., Riccobono, F., Rondo, L., Sarnela,  
622 N., Simon, M., Tomé, A., Tröstl, J., Winkler, P. M., Williamson, C., Ye, P., Curtius, J., Baltensperger,  
623 U., Donahue, N. M., Kulmala, M., and Worsnop, D. R.: Elemental composition and clustering



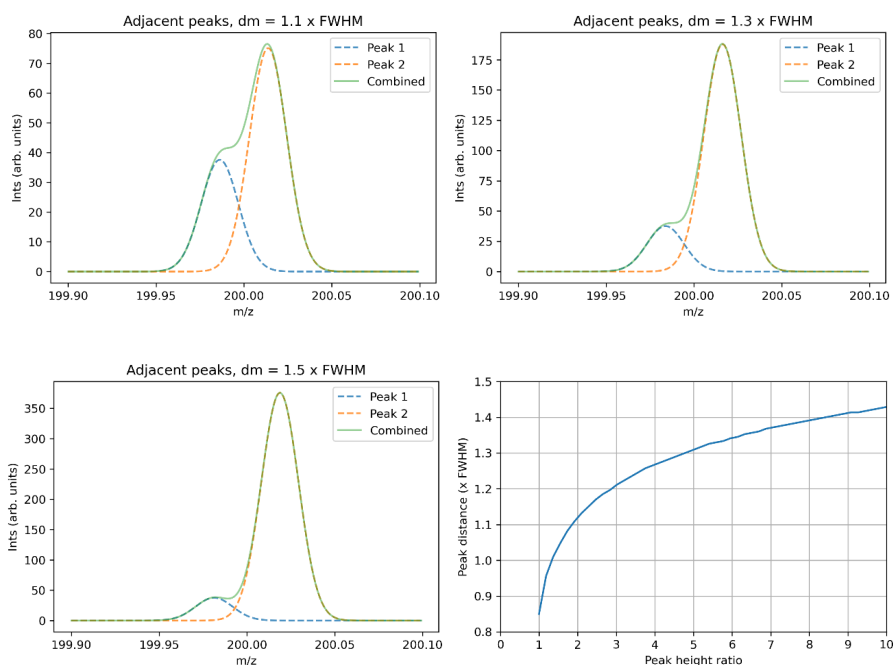
- 624 behaviour of  $\alpha$ -pinene oxidation products for different oxidation conditions, *Atmos. Chem. Phys.*,  
625 15, 4145-4159, 10.5194/acp-15-4145-2015, 2015.
- 626 Rissanen, M. P., Mikkilä, J., Iyer, S., and Hakala, J.: Multi-scheme chemical ionization inlet (MION)  
627 for fast switching of reagent ion chemistry in atmospheric pressure chemical ionization mass  
628 spectrometry (CIMS) applications, *Atmos. Meas. Tech.*, 12, 6635-6646, 10.5194/amt-12-6635-2019,  
629 2019.
- 630 Rissanen, M. P., Kurten, T., Sipilä, M., Thornton, J. A., Kangasluoma, J., Sarnela, N., Junninen, H.,  
631 Jorgensen, S., Schallhart, S., Kajos, M. K., Taipale, R., Springer, M., Mentel, T. F., Ruuskanen, T.,  
632 Petaja, T., Worsnop, D. R., Kjaergaard, H. G., and Ehn, M.: The formation of highly oxidized  
633 multifunctional products in the ozonolysis of cyclohexene, *J. Am. Chem. Soc.*, 136, 15596-15606,  
634 10.1021/ja507146s, 2014.
- 635 Riva, M., Brüggemann, M., Li, D., Perrier, S., George, C., Herrmann, H., and Berndt, T.: Capability of  
636 CI-Orbitrap for Gas-Phase Analysis in Atmospheric Chemistry: A Comparison with the CI-API-TOF  
637 Technique, *Anal. Chem.*, 92, 8142-8150, 10.1021/acs.analchem.0c00111, 2020.
- 638 Riva, M., Ehn, M., Li, D., Tomaz, S., Bourgain, F., Perrier, S., and George, C.: CI-Orbitrap: An  
639 Analytical Instrument To Study Atmospheric Reactive Organic Species, *Anal. Chem.*, 91, 9419-9423,  
640 10.1021/acs.analchem.9b02093, 2019a.
- 641 Riva, M., Rantala, P., Krechmer, J. E., Peräkylä, O., Zhang, Y., Heikkinen, L., Garmash, O., Yan, C.,  
642 Kulmala, M., Worsnop, D., and Ehn, M.: Evaluating the performance of five different chemical  
643 ionization techniques for detecting gaseous oxygenated organic species, *Atmos. Meas. Tech.*, 12,  
644 2403-2421, 10.5194/amt-12-2403-2019, 2019b.
- 645 Schobesberger, S., Junninen, H., Bianchi, F., Lonn, G., Ehn, M., Lehtipalo, K., Dommen, J., Ehrhart, S.,  
646 Ortega, I. K., Franchin, A., Nieminen, T., Riccobono, F., Hutterli, M., Duplissy, J., Almeida, J.,  
647 Amorim, A., Breitenlechner, M., Downard, A. J., Dunne, E. M., Flagan, R. C., Kajos, M., Keskinen,  
648 H., Kirkby, J., Kupc, A., Kurten, A., Kurten, T., Laaksonen, A., Mathot, S., Onnela, A., Praplan, A.  
649 P., Rondo, L., Santos, F. D., Schallhart, S., Schnitzhofer, R., Sipilä, M., Tome, A., Tsagkogeorgas,  
650 G., Vehkamäki, H., Wimmer, D., Baltensperger, U., Carslaw, K. S., Curtius, J., Hansel, A., Petaja,  
651 T., Kulmala, M., Donahue, N. M., and Worsnop, D. R.: Molecular understanding of atmospheric  
652 particle formation from sulfuric acid and large oxidized organic molecules, *Proc. Natl. Acad. Sci. U.*  
653 *S. A.*, 110, 17223-17228, 10.1073/pnas.1306973110, 2013.
- 654 Simon, M., Dada, L., Heinritzi, M., Scholz, W., Stolzenburg, D., Fischer, L., Wagner, A. C., Kürten, A.,  
655 Rörup, B., He, X.-C., Almeida, J., Baalbaki, R., Baccarini, A., Bauer, P. S., Beck, L., Bergen, A.,  
656 Bianchi, F., Bräkling, S., Brilke, S., Caudillo, L., Chen, D., Chu, B., Dias, A., Draper, D. C., Duplissy,  
657 J., El-Haddad, I., Finkenzeller, H., Frege, C., Gonzalez-Carracedo, L., Gordon, H., Granzin, M.,  
658 Hakala, J., Hofbauer, V., Hoyle, C. R., Kim, C., Kong, W., Lamkaddam, H., Lee, C. P., Lehtipalo,  
659 K., Leiminger, M., Mai, H., Manninen, H. E., Marie, G., Marten, R., Mentler, B., Molteni, U.,  
660 Nichman, L., Nie, W., Ojdanic, A., Onnela, A., Partoll, E., Petäjä, T., Pfeifer, J., Philippov, M.,  
661 Quéléver, L. L. J., Ranjithkumar, A., Rissanen, M. P., Schallhart, S., Schobesberger, S., Schuchmann,  
662 S., Shen, J., Sipilä, M., Steiner, G., Stozhkov, Y., Tauber, C., Tham, Y. J., Tomé, A. R., Vazquez-  
663 Pufleau, M., Vogel, A. L., Wagner, R., Wang, M., Wang, D. S., Wang, Y., Weber, S. K., Wu, Y.,  
664 Xiao, M., Yan, C., Ye, P., Ye, Q., Zauner-Wieczorek, M., Zhou, X., Baltensperger, U., Dommen, J.,  
665 Flagan, R. C., Hansel, A., Kulmala, M., Volkamer, R., Winkler, P. M., Worsnop, D. R., Donahue, N.



- 666 M., Kirkby, J., and Curtius, J.: Molecular understanding of new-particle formation from  $\alpha$ -pinene  
667 between  $-50$  and  $+25$  °C, *Atmos. Chem. Phys.*, 20, 9183-9207, 10.5194/acp-20-9183-2020, 2020.
- 668 Stolzenburg, D., Fischer, L., Vogel, A. L., Heinritzi, M., Schervish, M., Simon, M., Wagner, A. C.,  
669 Dada, L., Ahonen, L. R., Amorim, A., Baccarini, A., Bauer, P. S., Baumgartner, B., Bergen, A.,  
670 Bianchi, F., Breitenlechner, M., Brilke, S., Mazon, S. B., Chen, D., Dias, A., Draper, D. C., Duplissy,  
671 J., Haddad, I. E., Finkenzeller, H., Frege, C., Fuchs, C., Garmash, O., Gordon, H., He, X., Helm, J.,  
672 Hofbauer, V., Hoyle, C. R., Kim, C., Kirkby, J., Kontkanen, J., Kürten, A., Lampilahti, J., Lawler,  
673 M., Lehtipalo, K., Leiminger, M., Mai, H., Mathot, S., Mentler, B., Molteni, U., Nie, W., Nieminen,  
674 T., Nowak, J. B., Ojdanic, A., Onnela, A., Passananti, M., Petäjä, T., Quéléver, L. L. J., Rissanen, M.  
675 P., Sarnela, N., Schallhart, S., Tauber, C., Tomé, A., Wagner, R., Wang, M., Weitz, L., Wimmer, D.,  
676 Xiao, M., Yan, C., Ye, P., Zha, Q., Baltensperger, U., Curtius, J., Dommen, J., Flagan, R. C., Kulmala,  
677 M., Smith, J. N., Worsnop, D. R., Hansel, A., Donahue, N. M., and Winkler, P. M.: Rapid growth of  
678 organic aerosol nanoparticles over a wide tropospheric temperature range, *Proc. Natl. Acad. Sci. U.*  
679 *S. A.*, 115, 9122-9127, doi:10.1073/pnas.1807604115, 2018.
- 680 Surdu, M., Lamkaddam, H., Wang, D. S., Bell, D. M., Xiao, M., Lee, C. P., Li, D., Caudillo, L., Marie,  
681 G., Scholz, W., Wang, M., Lopez, B., Piedehierro, A. A., Ataei, F., Baalbaki, R., Bertozzi, B., Bogert,  
682 P., Brasseur, Z., Dada, L., Duplissy, J., Finkenzeller, H., He, X.-C., Höhler, K., Korhonen, K.,  
683 Krechmer, J. E., Lehtipalo, K., Mahfouz, N. G. A., Manninen, H. E., Marten, R., Massabò, D.,  
684 Mauldin, R., Petäjä, T., Pfeifer, J., Philippov, M., Rörup, B., Simon, M., Shen, J., Umo, N. S., Vogel,  
685 F., Weber, S. K., Zauner-Wieczorek, M., Volkamer, R., Saathoff, H., Möhler, O., Kirkby, J.,  
686 Worsnop, D. R., Kulmala, M., Stratmann, F., Hansel, A., Curtius, J., Welti, A., Riva, M., Donahue,  
687 N. M., Baltensperger, U., and El Haddad, I.: Molecular Understanding of the Enhancement in  
688 Organic Aerosol Mass at High Relative Humidity, *Environ. Sci. Technol.*, 57, 2297-2309,  
689 10.1021/acs.est.2c04587, 2023.
- 690 Trostl, J., Chuang, W. K., Gordon, H., Heinritzi, M., Yan, C., Molteni, U., Ahlm, L., Frege, C., Bianchi,  
691 F., Wagner, R., Simon, M., Lehtipalo, K., Williamson, C., Craven, J. S., Duplissy, J., Adamov, A.,  
692 Almeida, J., Bernhammer, A. K., Breitenlechner, M., Brilke, S., Dias, A., Ehrhart, S., Flagan, R. C.,  
693 Franchin, A., Fuchs, C., Guida, R., Gysel, M., Hansel, A., Hoyle, C. R., Jokinen, T., Junninen, H.,  
694 Kangasluoma, J., Keskinen, H., Kim, J., Krapf, M., Kurten, A., Laaksonen, A., Lawler, M.,  
695 Leiminger, M., Mathot, S., Mohler, O., Nieminen, T., Onnela, A., Petaja, T., Piel, F. M., Miettinen,  
696 P., Rissanen, M. P., Rondo, L., Sarnela, N., Schobesberger, S., Sengupta, K., Sipila, M., Smith, J. N.,  
697 Steiner, G., Tome, A., Virtanen, A., Wagner, A. C., Weingartner, E., Wimmer, D., Winkler, P. M.,  
698 Ye, P., Carslaw, K. S., Curtius, J., Dommen, J., Kirkby, J., Kulmala, M., Riipinen, I., Worsnop, D.  
699 R., Donahue, N. M., and Baltensperger, U.: The role of low-volatility organic compounds in initial  
700 particle growth in the atmosphere, *Nature*, 533, 527-531, 10.1038/nature18271, 2016.
- 701 Wang, M., Kong, W., Marten, R., He, X.-C., Chen, D., Pfeifer, J., Heitto, A., Kontkanen, J., Dada, L.,  
702 Kürten, A., Yli-Juuti, T., Manninen, H. E., Amanatidis, S., Amorim, A., Baalbaki, R., Baccarini, A.,  
703 Bell, D. M., Bertozzi, B., Bräkling, S., Brilke, S., Murillo, L. C., Chiu, R., Chu, B., De Menezes, L-  
704 P., Duplissy, J., Finkenzeller, H., Carracedo, L. G., Granzin, M., Guida, R., Hansel, A., Hofbauer,  
705 V., Krechmer, J., Lehtipalo, K., Lamkaddam, H., Lampimäki, M., Lee, C. P., Makhmutov, V., Marie,  
706 G., Mathot, S., Mauldin, R. L., Mentler, B., Müller, T., Onnela, A., Partoll, E., Petäjä, T., Philippov,  
707 M., Pospisilova, V., Ranjithkumar, A., Rissanen, M., Rörup, B., Scholz, W., Shen, J., Simon, M.,

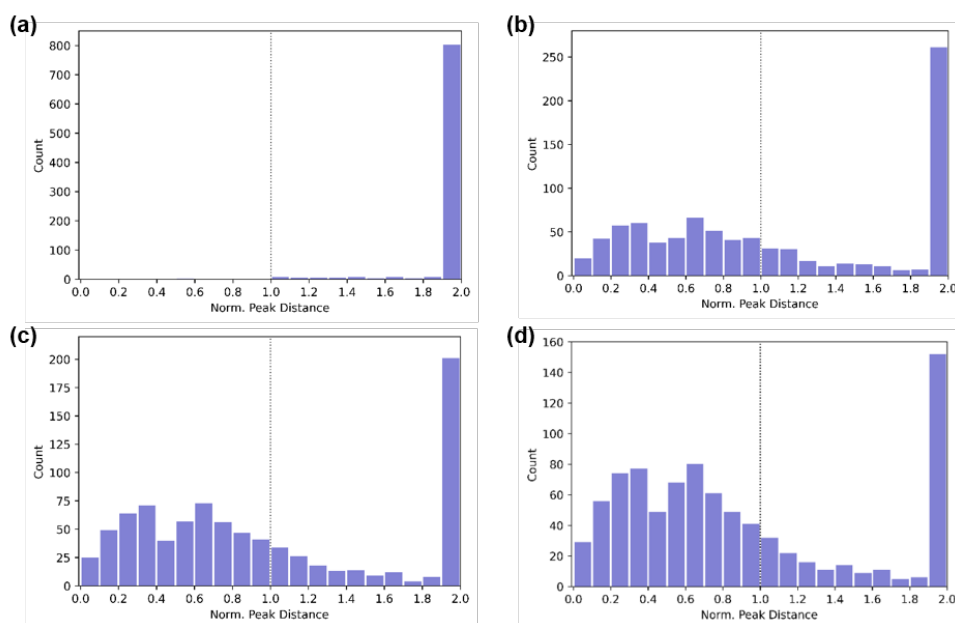


- 708 Sipilä, M., Steiner, G., Stolzenburg, D., Tham, Y. J., Tomé, A., Wagner, A. C., Wang, D. S., Wang,  
709 Y., Weber, S. K., Winkler, P. M., Wlasits, P. J., Wu, Y., Xiao, M., Ye, Q., Zauner-Wieczorek, M.,  
710 Zhou, X., Volkamer, R., Riipinen, I., Dommen, J., Curtius, J., Baltensperger, U., Kulmala, M.,  
711 Worsnop, D. R., Kirkby, J., Seinfeld, J. H., El-Haddad, I., Flagan, R. C., and Donahue, N. M.: Rapid  
712 growth of new atmospheric particles by nitric acid and ammonia condensation, *Nature*, 581, 184-189,  
713 10.1038/s41586-020-2270-4, 2020.
- 714 Wang, X., Hayeck, N., Brüggemann, M., Yao, L., Chen, H., Zhang, C., Emmelin, C., Chen, J., George,  
715 C., and Wang, L.: Chemical Characteristics of Organic Aerosols in Shanghai: A Study by Ultrahigh-  
716 Performance Liquid Chromatography Coupled With Orbitrap Mass Spectrometry, *J. Geophys. Res.-*  
717 *Atmos.*, 122, 11,703-711,722, 10.1002/2017jd026930, 2017.
- 718 Yuan, B., Koss, A. R., Warneke, C., Coggon, M., Sekimoto, K., and de Gouw, J. A.: Proton-Transfer-  
719 Reaction Mass Spectrometry: Applications in Atmospheric Sciences, *Chem. Rev.*, 117, 13187-13229,  
720 10.1021/acs.chemrev.7b00325, 2017.



723

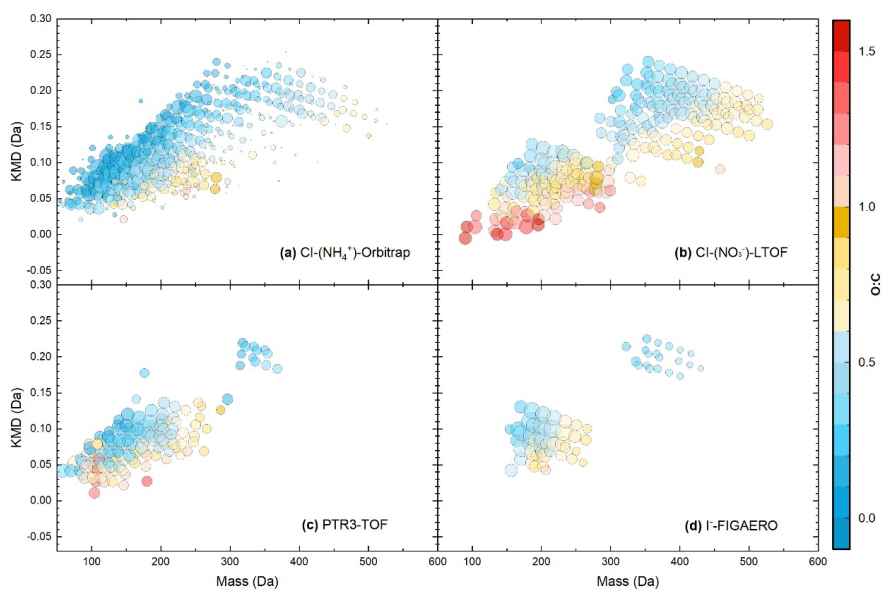
724 **Figure 1:** Simulated TOF spectra of overlapping peaks of equal intensity near  $m/z$  200 assuming a  
725 mass resolving power of 8,000, somewhere between that of a ToFwerk HTOF (“high-resolution time-  
726 of-flight”) and LTOF (“long high-resolution time-of-flight”) mass spectrometers. The overlapping area  
727 represents a greater proportion of the peak area of the less intense peak. Noise wasn’t added to the  
data.



728

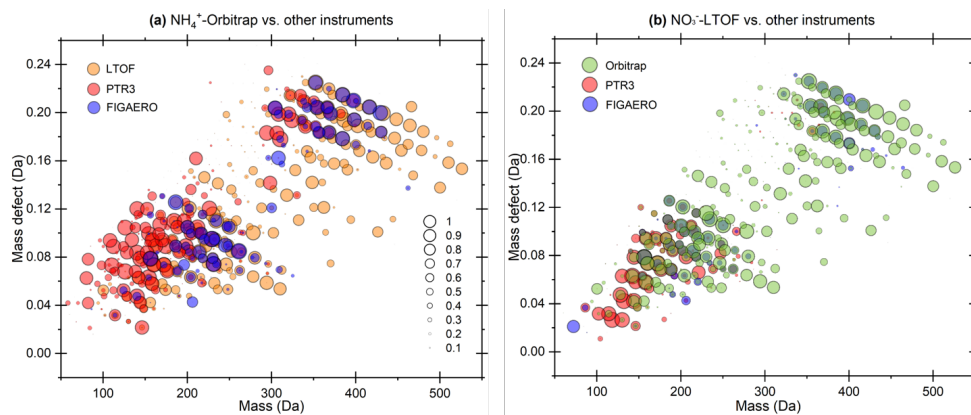
729 **Figure 2:** Distance of neighboring peaks normalized to the FWHM, which is a function of the mass  
730 resolving power of the mass analyzer and the nominal mass of the ion. For each ion, the distance to the  
731 closest neighbor with a relative peak intensity that exceeds 20%, 50%, or 100% is recorded. The  
732 average mass spectra observed during Run 2213 by the  $\text{NH}_4^+$ -Orbitrap is used to generate the analysis.  
733 (a) Orbitrap mass analyzer (mass resolution  $\sim 140,000$ )  $>99\%$  of ions are separated by at least 1  
734 FWHM from their neighbors with relative intensity threshold being set at 20%. (b) TOF mass analyzer  
735 (mass resolution  $\sim 10,000$ )  $>46\%$  of ions are separated by at least 1 FWHM from their neighbors with  
736 a relative intensity threshold being set at 100%. (c) TOF mass analyzer  $>39\%$  of ions are separated by  
737 at least 1 FWHM from their neighbors with a relative intensity threshold is set at 50%. (d) TOF mass  
738 analyzer  $>32\%$  of ions are separated by at least 1 FWHM from their neighbors with a relative intensity  
739 threshold is set at 20%.





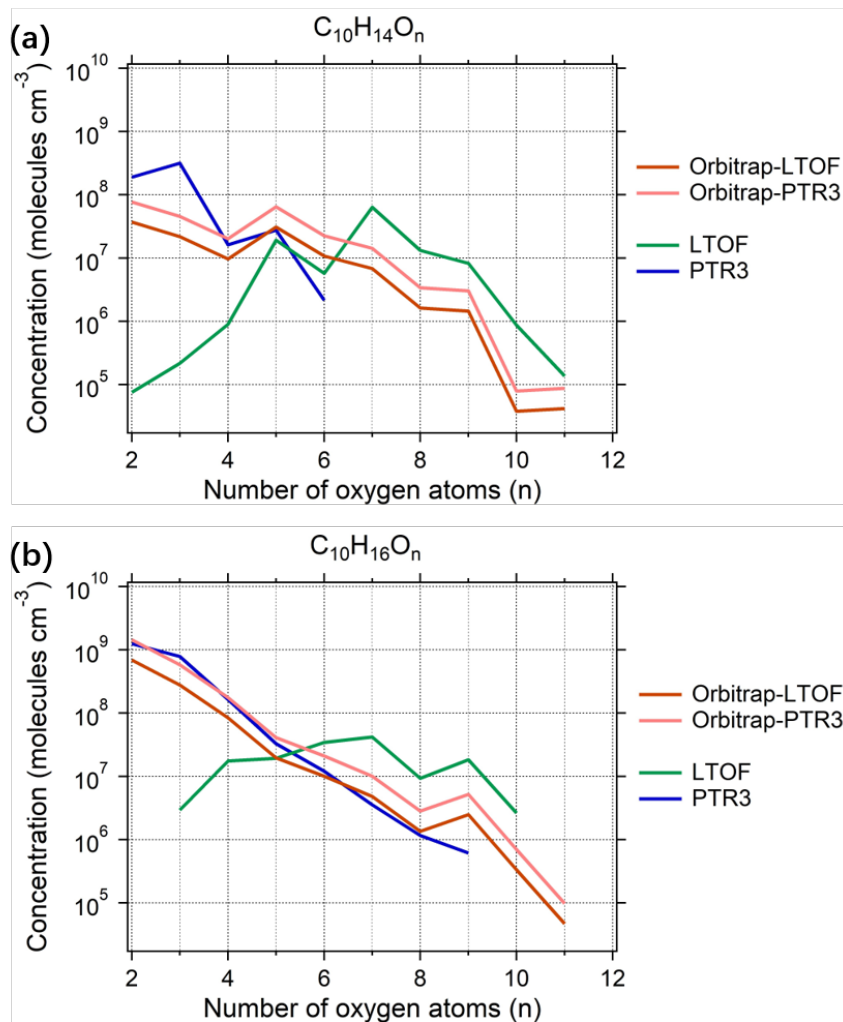
740

741 **Figure 3:** Mass defect plots for organic compounds measured by (a) CI-(NH<sub>4</sub><sup>+</sup>)-Orbitrap, (b) CI-  
742 (NO<sub>3</sub><sup>-</sup>)-LTOF, (c) PTR3-TOF and (d) I-FIGAERO-CIMS in run 2211. The x-axis represents the  
743 mass-to-charge ratio of the neutral analyte and the y-axis represents the corresponding mass defect,  
744 which is the difference between their exact mass and nominal mass (Schobesberger et al., 2013).  
745 Markers were all sized by the logarithm of their corresponding signals and colored by the O:C value.



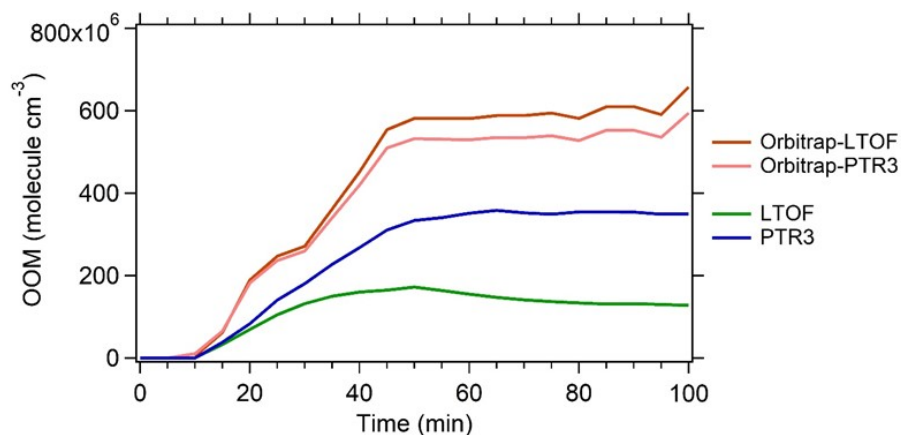
746

747 **Figure 4:** Mass defect plots depicting the compounds of which time series correlation was observed  
748 by (a) CI-(NH<sub>4</sub><sup>+</sup>)-Orbitrap and (b) CI-(NO<sub>3</sub><sup>-</sup>)-LTOF with other MS instruments. Each circle represents  
749 a molecule and marker size represents the correlation R<sup>2</sup> of time series of the molecule between two  
750 different MS instruments. Two sets of data in run 2211 and 2213 were used to reduce uncertainties.



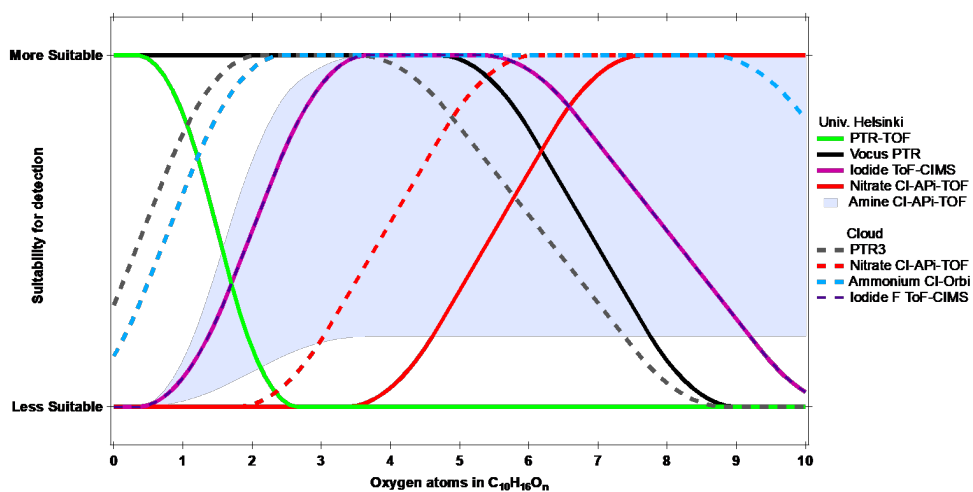
751

752 **Figure 5:** Estimated concentrations of the main  $C_{10}$ -monomer oxidation products observed in run  
753 2211.



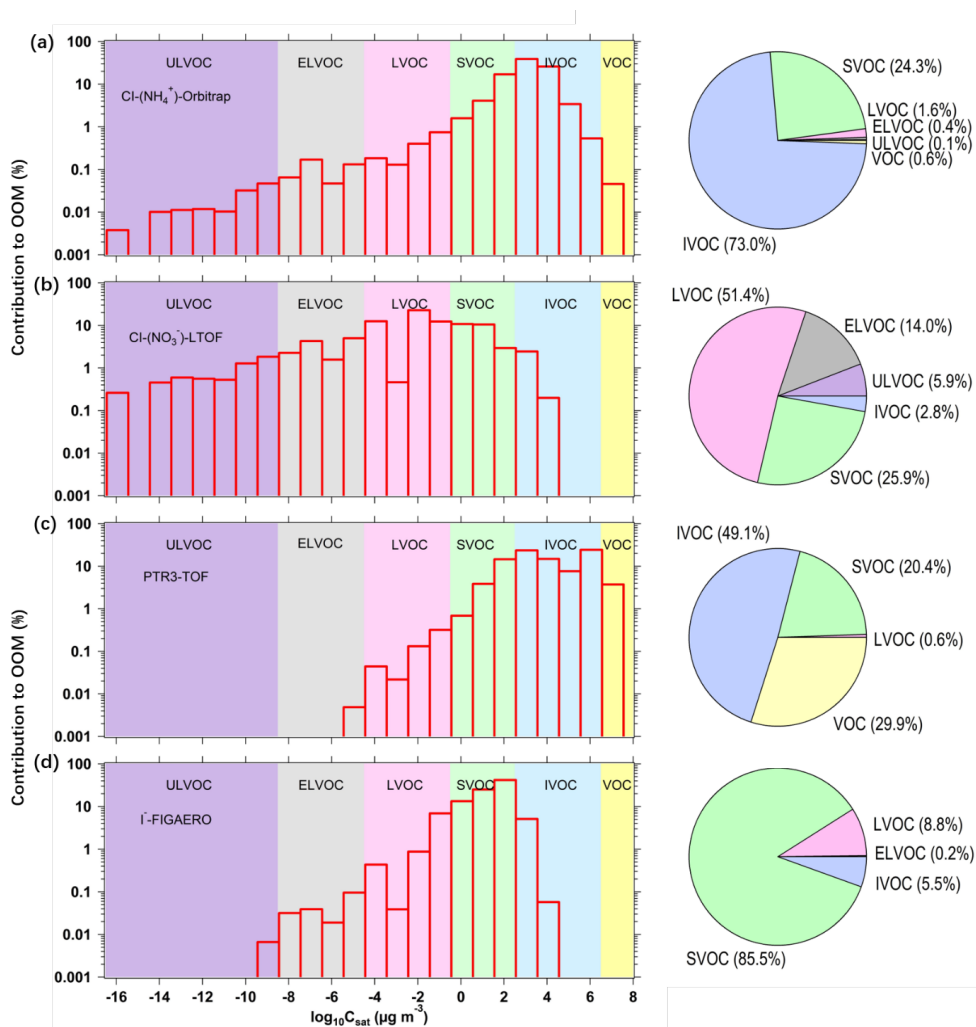
754

755 **Figure 6:** Estimated concentrations of all measured OOMs in the photooxidation of  $\alpha$ -pinene. All  
756 monomers  $C_{8-10}$  and dimers  $C_{18-20}$  measured by  $CI-(NH_4^+)$ -Orbitrap,  $CI-(NO_3^-)$ -LTOF, and PTR3-TOF  
757 in run 2213 were summed up. The concentrations of OOM measured by  $NH_4^+$ -Orbitrap were  
758 quantified by the calibration factors derived from correlation analysis between  $NH_4^+$ -Orbitrap and  
759  $NO_3^-$ -LTOF (Orbitrap-LTOF, light green) or PTR3-TOF (Orbitrap-PTR3, light blue), respectively.



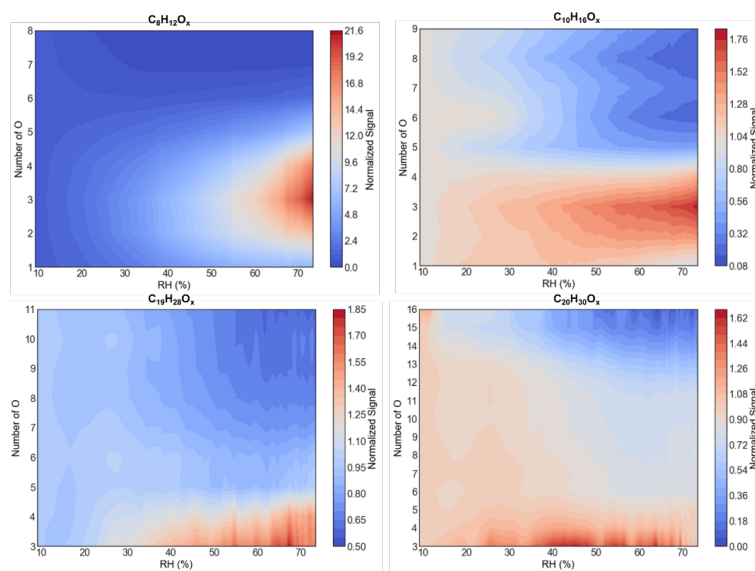
760

761 **Figure 7:** Estimated detection suitability of the different CIMS techniques for monomers from  $\alpha$ -  
762 pinene ozonolysis, plotted as a function of the number of oxygen atoms. Image modified from Riva et  
763 al.(Riva et al., 2019b).



764

765 **Figure 8:** Volatility distribution comparison for organic compounds detected by (a) CI-(NH<sub>4</sub><sup>+</sup>)-  
 766 Orbitrap, (b) CI-(NO<sub>3</sub><sup>-</sup>)-LTOF, (c) PTR3-TOF and (d) I-FIGAERO-CIMS. The background colors  
 767 represent the saturation concentration ( $C_{\text{sat}}$ ) in the range of ultra-low volatility (ULVOCs, purple),  
 768 extremely low volatility (ELVOCs, gray), low volatility (LVOCs, pink), semi-volatile (SVOCs,  
 769 green), intermediate volatility (IVOCs, blue) and volatile organic compounds (VOCs). The right pie  
 770 charts are the corresponding contributions of VOC, IVOC, SVOC, LVOC, ELVOC, and ULVOC  
 771 classes in run 2211.



772

773 **Figure 9:** The effect of relative humidity on the distribution of the most abundant monomers and  
774 dimers measured by  $\text{NH}_4^+$ -Orbitrap. The RH ramped from ~10% to ~80% in run 2211. The normalized  
775 signal represents the signal variation ratio at certain RH compared to that at RH = 10%, normalized

776 
$$\text{signal} = \frac{\text{signal}_{RH}}{\text{signal}_{10\%}}$$